

ANALOG VS DIGITAL: TESTING THE COMPARABILITY AND COMPATIBILITY OF
DICECT AND GROSS DISSECTION, WITH SPECIAL EMPHASIS ON MUSCLE TISSUE

A Thesis

Presented to

The Faculty of the Department of Biological Sciences

Sam Houston State University

In Partial Fulfillment

of the Requirements for the Degree of

Master of Science

by

Justin Levy

August, 2018

ANALOG VS DIGITAL: TESTING THE COMPARABILITY AND COMPATIBILITY OF
DICECT AND GROSS DISSECTION, WITH SPECIAL EMPHASIS ON MUSCLE TISSUE

by

Justin Levy

APPROVED:

Patrick J. Lewis, PhD
Thesis Director

Juan D. Daza, PhD
Committee Member

Justin K. Williams, PhD
Committee Member

Adam Hartstone-Rose, PhD
Committee Member

John B. Pascarella, PhD
Dean, College of Science and Engineering
Technology

ABSTRACT

Levy, Justin , *Analog vs digital: Testing the comparability and compatibility of diceCT and gross dissection, with special emphasis on muscle tissue*. Master of Science (Biology), August, 2018, Sam Houston State University, Huntsville, Texas.

Diffusible iodine-based contrast-enhanced computed tomography (diceCT) is a new tool in the study of anatomy. With diceCT, researchers can visualize *in situ* soft tissue, in three dimensional space. The relationship of these results to traditional gross dissection is unknown. Despite this, it has begun to be used for quantitative comparisons. This approach requires more research to determine the comparability of diceCT and gross dissection. To study the relationship of these two methods, the head of a common marmoset, *Callithrix jacchus*, was stained in 2.5% Lugol's solution (I₂KI) for 37 days. The head CT scanned for digital dissection prior to physical dissection. Amira 5.6 was used for digital segmentation to reconstruct connective, epithelial, muscle, and nervous tissues. Masses of muscle were taken for muscle density comparisons to the previously established mammalian muscle density constants. Based on Bland-Altman analyses, gross dissection and diceCT do not produce comparable measurements in all circumstances. Muscle and epithelial tissue, as well as volumetric measurements are significantly different between gross dissection and diceCT. Muscle densities were also found to be significantly different than previously established constants, through the use of one sample *t* tests. New, diceCT-calibrated constants are proposed for use with specimens that cannot be dissected. Muscle density is not constant, and should not be treated as such. This process is still widely beneficial when traditional destructive dissection is not possible. It allows for three dimensional views of structures that are not

otherwise visible due to size and/or morphology, however, comparisons between gross dissection and diceCT should be approached with caution.

KEY WORDS: Diffusible iodine-based contrast-enhanced computed tomography (diceCT), Gross dissection, Three-dimensional imaging, Comparison, Muscle density, *Callithrix jacchus*, Epithelial tissue, Muscle tissue, Volumetric data

ACKNOWLEDGEMENTS

First and foremost, I would like to thank my committee chair and advisor Dr. Patrick J. Lewis for his support and guidance in the completion of this thesis and my degree as a whole. I would also like to thank my other committee members from Sam Houston State University, Dr. Juan D. Daza, and Dr. Justin K. Williams, for their suggestions and guidance during the course of my studies and thesis writing. Dr. Adam Hartstone-Rose, my external committee member from North Carolina State University, has been instrumental in the conceiving and execution of this project, while greatly assisting in the writing process. I would also like to thank Carissa Leischner, from the University of South Carolina, for invaluable assistance during the gross dissection, and Joseph A. Costa, from the University of Buffalo, for his discussions on anatomy. For help learning how to get the most out of Amira, I'd like to thank Lauren Rudie, Christiana Fakhri, and Sarai Mesa, of Sam Houston State University, and Colin Basham, from the University of South Carolina. Thank you to Kelsey M. Jenkins for editing and valuable discussion that improved this thesis greatly, especially during the writing process. Finally, for always lifting me up and pushing me forward, thank you to my partner Cady Willems for helping me through this trying time, in which I've accomplished more than I ever thought possible. I would not have finished this without you.

This work was partially funded by Dr. Hartstone-Rose's grant from the National Science Foundation (IOS-15-57125).

TABLE OF CONTENTS

	Page
ABSTRACT.....	iii
ACKNOWLEDGEMENTS.....	v
TABLE OF CONTENTS.....	vi
LIST OF TABLES.....	viii
LIST OF FIGURES.....	ix
CHAPTER	
I LITERATURE REVIEW.....	1
History of Computed Tomography.....	1
Tissue.....	2
Specimen.....	3
Assumption of Comparability.....	3
Lack of Physical Dissection.....	8
Inappropriate Use of Scale Bars.....	8
Histology.....	9
Hypotheses.....	10
Significance.....	11
Literature Cited.....	12
II ANALOG VS DIGITAL: A COMPARATIVE STUDY BETWEEN DICECT AND GROSS DISSECTION.....	23
Abstract.....	24
Introduction.....	26

Methods.....	30
Results.....	35
Discussion.....	37
Conclusions.....	41
Acknowledgements.....	41
References.....	42
III A RECALIBRATION OF THE SPECIFIC DENSITY OF MUSCLE IN THE ERA OF DICECT.....	70
Abstract.....	71
Introduction.....	72
Methods.....	73
Results.....	76
Discussion.....	78
Conclusions.....	81
Acknowledgements.....	81
References.....	83
IV CONCLUSIONS.....	100
REFERENCES.....	102
APPENDIX.....	114
VITA.....	122

LIST OF TABLES

Table		Page
1	Scanning Parameters.....	50
2	Volume measurements by method.....	51
3	Mandible volumes and grayscale value data	52
4	Volumes and percentages of mastication muscles for gross dissection and diceCT.....	53
5	Muscles analyzed, including masses, volumes, and densities	88
6	Muscle density one sample t test results.....	96
7	Bland Altman analyses results	98

LIST OF FIGURES

Figure	Page
1 Side-by-side comparison of microCT (left) and diceCT (right) slices through the head of a <i>Callithrix jacchus</i>	21
2 Bland Altman analysis of data from Bribiesca-Contreras & Sellers 2017.	22
3 Common marmoset head used in study.	56
4 Example segmentation and rendering	57
5 Partially dissected common marmoset.....	58
6 Example Bland-Altman analyses.....	59
7 Bland Altman analysis of gross dissection (analog) compared to diceCT (digital) measurements.....	60
8 Bland Altman analysis of connective tissue data.....	61
9 Histogram comparison of grayscale values between the stained and unstained mandible.....	62
10 Bland Altman analysis of epithelial tissue measurements.....	63
11 Bland Altman analysis of muscle tissue measurements.	64
12 Bland Altman analysis of linear measurements.....	65
13 Muscle, gland, and mandible reconstructions.....	66
14 Bland Altman analysis of volumetric data.....	67
15 Bland Altman analysis of volumetric data obtained using Archimedes' method.....	68
16 Bland Altman analysis of volumetric data obtained using the specific muscle density method.....	69

17 Regression analysis of muscle density data. 99

CHAPTER I

Literature Review

Recently, researchers using diffusible iodine-based contrast-enhanced computed tomography (“diceCT”) (sensu Gignac et al. 2016) have generated biomechanical models for investigating a variety of medical, functional morphological, and phylogenetic questions (Metscher, 2009a,b; Cox et al. 2011, 2012; Cox & Jeffery, 2011; Baverstock et al. 2013; Cox & Faulkes, 2014; Vickerton et al. 2014; Herdina et al. 2015a; Clarke et al. 2016). As diceCT is proposed as a dissection alternative (Gignac et al. 2016), it must be tested against traditional gross dissection methods to evaluate equivalency in measurements generated. Here I will test how the data produced using diceCT compares to the data produced by traditional gross dissection, to assess the comparability of the two methods.

History of Computed Tomography

Computed tomography (CT) is increasingly used in biology and medical sciences, with microCT, a higher resolution of computed tomography, first introduced to analyze mineralized tissues (Elliot and Dover, 1982). While microCT continues to be a popular tool for analyzing mineralized tissues (e.g. Davis & Wong, 1996; Peters et al. 2000; Neues et al. 2007; Vasquez et al. 2008), more recently a variation of the method was introduced to analyze soft tissue (Metscher, 2009a,b). Since microCT does not distinguish soft tissue, a contrast agent is needed to enhance visualization of less radiopaque materials (Metscher, 2009a,b; *Figure 1*).

Several staining radiopaque compounds are used to enhance the contrast on CT scans including gallocyanin-chromalum (Metscher, 2009a,b), iodine in ethanol (e.g.

Faulwetter et al. 2013; Staedler et al. 2013; Dougherty et al. 2015), Lugol's iodine (e.g. Metscher, 2009a,b; Cox & Jeffery, 2011; Aslandi et al. 2013; Li et al. 2016;), osmium tetroxide (e.g. Mizutani & Suzuki, 2012; Pauwels et al. 2013), and phosphotungstic acid (e.g. Metscher, 2009a,b; Pauwels et al. 2013; Staedler et al. 2013). Iodine central methods, such as iodine in ethanol and Lugol's iodine, are the primary reagents used among current researchers (Gignac et al. 2016). Lugol's iodine, (I_2KI) improves visualization of muscle fibers, relative to the other main reagent, iodine in ethanol, or I_2E (Li et al. 2016).

DiceCT has been used to image organisms across the tree of life. The taxa on which this method is most commonly used on are birds (e.g. Metscher, 2009a; Gignac & Kley, 2014; Bribiesca-Contreras & Sellers, 2017) and mammals (e.g. Metscher, 2009b; Cox et al. 2011, 2012; Kupczik et al. 2015). Reptiles (e.g. Tsai & Holliday, 2011; Gignac & Kley, 2014), amphibians (e.g. Metscher, 2009b, Gignac et al. 2016), and insects (e.g. Metscher, 2009b; Zimmermann et al. 2011; Sombke et al. 2015) are studied less often. DiceCT is also used with ray-finned fish (Metscher, 2009b), lampreys (Metscher, 2009b), and invertebrates, including centipedes (Sombke et al. 2015), millipedes (Akkari et al. 2015) mollusks (Metscher, 2009b), oligochaetes (Fernández et al. 2013), polychaetes (Faulwetter et al. 2013), as well as plants (Staedler et al. 2013).

Tissue

The staining process can reveal all four types of tissue; connective, epithelial, muscular, and nervous (Gignac et al. 2016). Connective tissue is abundant and can be found in many forms in the body, including fat tissue, cartilage, bone, and dense tissue such as tendons and ligaments (Miller, 1898). Epithelial tissue lines cavities and hollow

structures, in addition to forming glands, and constituting the skin, which covers the body (Miller, 1898). Muscle tissue is sorted into three categories; the smooth, forming viscera, the skeletal, generally attached to bone and fasciae, and cardiac making the heart walls (Miller, 1898). Nervous tissue forms the brain, spinal cord, central and peripheral nervous systems (Miller, 1898).

Specimen

A New World monkey (Platyrrhini), the common marmoset (*Callithrix jacchus*), is the test specimen for this study. The specimen is small enough to be scanned, but also large enough to perform traditional gross dissection. Due to the propensity of diceCT research revolving around the head, it was selected to study. The use of the common marmoset head also appeals to physical anthropology researchers, as there is a focus on the skull and masticatory muscles.

The common marmoset is native to forests in northeastern Brazil, covering Piauí, Alagoas, Pernambuco, Paraíba, Ceará, Rio Grande do Norte, and the southeastern parts of Maranhão (Rylands et al. 1993, 2008; Fleagle, 2013). *Callithrix jacchus* is diurnal, spending much of its day foraging for its preferred diet of exudates (i.e. exuded substances), using its teeth to bore into trees to consume exudates such as gum and sap, while also feeding on insects and fruits (Rylands et al. 1993; Fleagle, 2013; Pinheiro & Pontes, 2015). This special feeding mechanism's relationship to cranial anatomy is a key reason a *Callithrix jacchus* specimen was chosen.

Assumption of Comparability

Traditional CT Comparability. Traditional CT produces statistically comparable linear measurements for bone (Loubele et al. 2006; Lagravere et al. 2008;

Periago et al. 2008; Brown et al. 2009; Moerenhout et al. 2009; Damstra et al. 2010; Güngör & Doğan, 2017; Yuen et al, 2017). Volume measurements for bone are also considered statistically comparable (Albuquerque et al. 2011; Whyms et al. 2013; Sang et al. 2016; Shaheen et al. 2017). However, these findings do not necessarily apply to diceCT, because the presence of soft tissue in scans may affect both linear and volumetric measurements of bone in CT (Dusseldorp et al. 2017). Those differences in linear and volumetric measurements may be more pronounced when using diceCT, because bone decreases in contrast when stained in Lugol's iodine (Metscher, 2009a; Cox & Jeffery, 2011; Baverstock et al. 2013; Gignac & Kley, 2014).

Inadequate Comparisons. Comparisons between diceCT and gross dissection do not show enough statistical support to be the sole support of the proposition that these methods produce insignificantly different measurements. Linear bone measurements in diceCT and histology have been reported, including average numbers that were similar, though not statistically evaluated (Herdina et al. 2010). However, Herdina et al. (2010) had different sample sizes for each dissection method and cannot be considered a direct comparison. The different sample sizes are problematic because it shows that there was not a one-to-one comparison of measurements, otherwise the sample sizes of both the diceCT and gross dissection would be equivalent. Average vessel diameters along the long and short axes in mice embryos were found to not be significantly different in diceCT and histological sections (Degenhardt et al. 2010), but the sample size was small (n=3). In another study, four mice were dissected physically and one digitally (Baverstock et al. 2013). No statistics were reported regarding data comparison, but the authors report that there seems to be no difference for volumes (Baverstock et al. 2013).

A comparison between automated fascicle diceCT calculations, and gross dissection for pennation angles, and fascicle lengths has also been performed (Kupczik et al. 2015). Pennation angles were found to be significantly different between the gross dissection and digital dissection, as were fascicle lengths before a selective correction was applied (Kupczik et al. 2015). Automated fascicle measurements then seem to be statistically similar, but it is not a direct comparison, as fascicles and pennation angle averages were computed and compared (Kupczik et al. 2015). An average cannot be a true one-to-one comparison of the measurements. A one-to-one comparison is necessary to ensure that the same structures are measured, removing a degree of uncertainty from the statistical analysis.

One-to-One Comparisons. Only three studies performed true one-to-one comparisons, measuring the same structures in both diceCT and traditional gross dissection (Vickerton et al. 2013; Bribiesca-Contreras & Sellers, 2017; Santana, 2018). A dissection was unnecessary in the first study (Vickerton et al. 2013), as all structures were analyzed *ex vivo*. The main goal of the study was to look at the amount of shrinkage seen due to different staining strengths of Lugol's iodine (Vickerton et al. 2013). The results come with a strong caveat; they were focused on isolated muscles, and it is suggested that there is likely less shrinkage when muscles are *in situ* (Vickerton et al. 2013). The volumes of the muscles, when measured, were not significantly different from the diceCT muscle volume measurements (Vickerton et al. 2013). This was established by means of a linear regression (Vickerton et al. 2013), but this method is considered an inappropriate standard by which to compare two methods (Ludbrook, 1997; Giavarina, 2015), with a Bland-Altman analysis preferred (Altman and Bland, 1983). The second study that

performed a one-to-one comparison (Bribiesca-Contreras & Sellers, 2017), also used a linear regression to determine the comparability of the 3D model measurements to the gross dissection measurements. Due to a high correlation, it was concluded that the two methods are comparable (Bribiesca-Contreras & Sellers, 2017). Using the data from Bribiesca-Contreras & Sellers (2017), a high correlation coefficient ($r=0.981$; *Figure 2*) is obtained, these methods would not be considered comparable by the general standard for Bland-Altman analyses (Critchley & Critchley, 1999; *Figure 2*). The mean percent difference in the two methods was 7.28%, meaning diceCT measurements were larger than their counterparts from gross dissection, on average (*Figure 2*). The 95% confidence intervals around the mean run from 113.3% to -98.74%, well outside of the $\pm 30\%$ interval set forth by Critchley & Critchley (1999). Bribiesca-Contreras & Sellers (2017) de-stained their specimen prior to obtaining the masses of the muscles, which were used calculate volume. This could have led to the overestimation in diceCT, as some mass and volume may have been lost during de-staining, or due to the estimation of volume from mass. Physiological cross-sectional areas produced from diceCT and traditional gross dissection were found to be significantly different (Santana, 2018). The lack of comparative studies between gross dissection and diceCT provides potential problems, for example, many studies (Herdina et al. 2010; Cox & Jeffery 2011; Cox et al. 2012; Stephenson et al. 2012; Wong et al. 2012, 2013; Cox & Faulkes, 2014; Vickerton et al. 2014; Kupczik et al. 2015, Sombke et al. 2015) compare their quantitative data to the literature using potentially inequivalent or incomparable data, which could lead to misinformed conclusions. These comparisons are made with both traditional gross dissection measurements (e.g. Kupczik et al. 2015) and diceCT measurements (e.g. Cox

& Faulkes, 2014 compared to Cox & Jeffery, 2011), making it more difficult to assess the validity of conclusions. By combining data from published studies with their own digital data, biomechanical models were produced (Vickerton et al. 2014). Other researchers provide linear data (Degenhardt et al. 2010; Akkari et al. 2015; Herdina et al. 2015b; Kupczik et al. 2015), volumetric data (Wong et al. 2012, 2014; Baverstock et al. 2013; Vickerton et al. 2014), or both (Cox & Jeffery, 2011; Stephenson et al. 2012; Holliday et al. 2013; Cox & Faulkes, 2014; Sombke et al. 2015; Bribiesca-Contreras & Sellers, 2017) explicitly from diceCT measurements, which, if not comparable, may lead other researchers to invalid conclusions. Some published 3D pdfs containing data (Düring et al. 2013; Holliday et al. 2013; Lautenschlager et al. 2013; Cox & Faulkes, 2014; Herdina et al. 2015a; Sombke et al. 2015; Clarke et al. 2016), which has not been shown to be equivalent. Mixed data methods (i.e. when authors use multiple methods to complement one another) could also present issues regarding model building and comparisons using diceCT. Mixed data methods assume equivalency, though the two methods have yet to be shown as equivalent in the literature. A project interested in bite force analysis generated from diceCT methods reported comparable results to maximum force obtained through *in vivo* testing (Cox et al. 2012). However, those measurements came from different specimens than those that underwent diceCT, and were based on averages (Cox et al. 2012). While it is standard and understandable to not kill animals that behavioral data was collected from, it is not as ideal as comparing the bite force directly to the animal that provided the measure. Another diceCT study performed dissections on the heads of an alligator and an emu, but reported no specific data (e.g. volumetric, lengths, widths, heights, etc.) from the dissections (Gignac & Kley, 2014).

Lack of Physical Dissection

In many cases of diceCT, no physical dissections were performed to be used for direct comparison to diceCT methods (e.g. Degenhardt et al. 2010; Cox et al. 2011, 2012; Hautier, et al. 2012; Anderson & Maga, 2015). Some researchers discuss the difficulty of measuring exceedingly small objects in dissection as support for using diceCT (e.g. Stephenson et al. 2012; Lautenschlager et al. 2013; Herdina et al. 2015b). Without physical dissections, diceCT cannot be evaluated for comparison with gross dissection.

Inappropriate Use of Scale Bars

Many studies include scale bars on digital models, without explicit comparison statistics or any support to their validity (e.g. Metscher, 2009a,b, 2013; Wong et al. 2012, 2013, 2014; Sombke et al. 2015; Hughes et al. 2016). When physical specimens are unable to be obtained it is not uncommon to use specimen images to generate characters for phylogenetic analysis (Seymour, 1999; Ramírez et al. 2007). Three dimensional pdfs that allow for direct interaction and measurements of specimens have been published, in part, with these goals in mind (Düring et al. 2013; Holliday et al. 2013; Lautenschlager et al. 2013; Cox & Faulkes, 2014; Herdina et al. 2015a; Sombke et al. 2015; Clarke et al. 2016). Unfortunately, some do not activate properly to allow interaction (Clarke et al, 2016), while others have no specified units (Düring et al. 2013; Sombke et al. 2015), or are not properly calibrated (Düring et al. 2013; Lautenschlager et al. 2013; Herdina et al. 2015a), resulting in inflated measurements. One of the models read as over 100 mm for a measurement that should have been approximately 1 mm according to the scale bars (Düring et al. 2013). Other models' measurements were over 1 m for both a common buzzard skull and a bat baculum (Lautenschlager et al. 2013; Herdina et al. 2015a). These

3D pdfs have to be calibrated by the original author, otherwise these errors will happen. They can be corrected by redefining the model units, which were not provided in the 3D pdfs with calibration errors (Düring et al. 2013; Lautenschlager et al. 2013; Herdina et al. 2015a). In these cases, there was an error and the 3D pdf needs to be recalibrated, but it may not always be evident that a mistake has been made. If the digital model measurements prove to be incomparable to gross dissection, the resultant models, which are typically based off gross dissection, may be compromised, ultimately affecting the conclusions drawn.

Histology

Histological methods have been used for direct comparison to diceCT, but only qualitatively (Jeffery et al. 2011; Stephenson et al. 2012; Herdina et al. 2015b). Despite no reports of measurements or statistical analysis between the datasets, they were deemed to be correlated. Light microscopy histological sections were compared to diceCT directly for three bat penes, looking particularly at bacula, determining that the methods were comparable to histology qualitatively, however, there was no statistical analysis or published quantitative dissection data, save for scale bars (Herdina et al. 2015b).

Histology was performed only on a small sample of tissue that also underwent diceCT, but they were compared for the qualitative purpose of determining if diceCT allowed for the same delineation of fascicles that histology allows (Jeffrey et al. 2011). Histology has also been used to focus on qualitatively comparing the ability of diceCT to visualize the cardiac conduction system in rat hearts (Stephenson et al. 2012). Histology has also been used as an indirect, qualitative, comparison to diceCT, meaning different specimens from those that underwent diceCT were histologically prepared (Degenhardt et al. 2010;

Herdina et al. 2010; Tsai & Holliday, 2011; Taraha & Larsson, 2013; Wong et al. 2013; Vickerton et al. 2014).

After reviewing the literature, it has become apparent that a comparative study between the traditional gross dissection and digital dissection based on diceCT would yield valuable information about the comparability and compatibility of these methods.

Hypotheses

Null Hypothesis: Measurements obtained from gross dissection and diceCT on a *Callithrix jacchus* specimen will not be significantly different. The following sub-hypotheses will seek to clearly delineate if the null hypothesis is supported for all measurements:

1: Measurements will not be significantly different between gross dissection and diceCT for connective tissue.

2: Measurements in bone will not be significantly different for CT, diceCT and gross dissection.

3: Measurements will not be significantly different between gross dissection and diceCT for epithelial tissue.

4: Measurements will not be significantly different between gross dissection and diceCT for nervous tissue.

5: Measurements will not be significantly different between gross dissection and diceCT for muscle tissue.

6: Linear measurements will not be significantly different between gross dissection and diceCT.

7: Volumetric measurements will not be significantly different between gross dissection and diceCT.

These hypotheses are being tested as they are the working assumptions that all previous researchers in the field have used.

Significance

This research will help to determine the compatibility of the diceCT dissection to traditional gross dissection by looking at all four tissue types: epithelial, connective, muscular, and nervous. Due to the diversity of the data set, this research should be helpful to many different sub-disciplines, from those who study sight and want to better visualize the internal structures of the eye, to those that study muscle fiber architecture by looking at individual fascicles. Via pennation angles and fascicle lengths for biomechanical modeling, as well as digital atlases, this method has already begun to take hold, but it needs to be supported. Now it will be able to be used with more certainty that the measurements returned are comparable to those from gross dissection. DiceCT measurements are already being compared with those from gross dissection. This study will determine if those comparisons previously done are appropriate, and give future works a more solid footing from which to start.

Literature Cited

- Albuquerque MA, Gaia BF, Cavalcanti MG.** (2011) Comparison between multislice and cone-beam computerized tomography in the volumetric assessment of cleft palate. *Oral Surg Oral Med Oral Pathol Oral Radiol Endod* **112(2)**, 249-257.
- Akkari N, Enghoff H, Metscher BD.** (2015) A new dimension in documenting new species: High-detail imaging of myriapod taxonomy and first 3D cybertype of a new millipede species (Diplopoda, Julida, Julidae). *PLoS ONE* **10(8)**: e0135243.
- Altman DG, Bland JM.** (1983) Measurement in medicine: The analysis of method comparison studies. *J R Stat Soc* **32**, 307-317.
- Anderson R, Maga AM.** (2015) A novel procedure for rapid imaging of adult mouse brains with microCT using iodine-based contrast. *PLoS ONE* **10(11)**: e0142974.
- Aslandi OV, Nikolaidou T, Zhao J, et al.** (2013) Application of micro-computed tomography with iodine staining to cardiac imaging, segmentation and computational model development. *IEEE Trans Med Imaging* **32(1)**, 8-17.
- Baverstock H, Jeffery NS, Cobb SN** (2013) The morphology of the mouse masticatory musculature. *J Anat* **223**, 46–60.
- Bribiesca-Contreras F, Sellers WI.** (2017) Three-dimensional visualization of the internal anatomy of the sparrowhawk (*Accipiter nisus*) forelimb using contrast-enhanced micro-computed tomography. *PeerJ* **5**: e3039.
- Brown AA, Scarfe WC, Scheetz JP, et al.** (2009) Linear accuracy of cone beam CT derived 3D images. *Angle Orthod* **79(1)**, 150-157.
- Clarke JA, Chatterjee S, Li Z, et al.** (2016) Fossil evidence of the avian vocal organ from the Mesozoic. *Nature* **538**, 502–505

- Cox PG, Fagan MJ, Rayfield EJ, et al.** (2011) Finite element modeling of squirrel, guinea pig and rat skulls: using geometric morphometrics to assess sensitivity. *J Anat* **219**, 696–709.
- Cox PG, Faulkes CG.** (2014) Digital dissection of the masticatory muscles of the naked mole-rat, *Heterocephalus glaber* (Mammalia, Rodentia). *PeerJ* **2**, e448.
- Cox PG, Jeffery N.** (2011) Reviewing the morphology of the jaw-closing musculature in squirrels, rats, and guinea pigs with contrast-enhanced micro-CT. *Anat Rec* **294**, 915–928.
- Cox PG, Rayfield EJ, Fagan MJ, et al.** (2012) Functional evolution of the feeding system in rodents. *PLoS ONE* **7**, e36299.
- Critchley LAH, Critchley AJH.** (1999) A meta-analysis of studies using bias and precision statistics to compare cardiac output measurement techniques. *J Clin Monit Comput* **15(2)**, 85-91.
- Damstra J, Fourie Z, Huddleston Slater JJR, et al.** (2010) Accuracy of linear measurements from cone-beam computed tomography-derived surface models of different voxel sizes. *Am J Orthod Dentofacial Orthop* **137**, 16.e1-16.e6.
- Davis GR, Wong FS.** (1996) X-ray microtomography of bone and teeth. *Physiol Meas* **17**, 121-146.
- Degenhardt K, Wright AC, Horng D, et al.** (2010) Rapid 3D phenotyping of cardiovascular development in mouse embryos by micro-CT with iodine staining. *Circ Cardiovasc Imaging* **2010(3)**, 314-322.

- Dougherty LR, Rahman IA, Burdfield-Steel ER, et al.** (2015) Experimental reduction of intermittent organ length reduces male reproductive success in a bug. *Proc Roy Soc Lond B* **282**, 20150724
- Düring DN, Ziegler A, Thompson CK, et al.** (2013) The songbird syrinx morphome: a three-dimensional, high-resolution, interactive morphological map of the zebra finch vocal organ. *BMC Biol* **11**, 1.
- Dusseldorp JK, Stamatakis HC, Ren Y.** (2017) Soft tissue coverage on the segmentation accuracy of the 3D surface-rendered model from cone-beam CT. *Clin Oral Invest* **21**, 921-930.
- Elliot JC, Dover SD.** (1982) X-ray microtomography. *J Microsc* **126(2)**, 211-213.
- Faulwetter S, Vasileiadou A, Kouratoras M, et al.** (2013) Micro-computed tomography: Introducing new dimensions to taxonomy. *Zookeys* **263**, 1-45.
- Fernández R, Kvist S, Lenihan J, et al.** (2014) Sine systemate chaos? A versatile tool for earthworm taxonomy: non-destructive imaging of freshly fixed and museum specimens using micro-computed tomography. *PLoS ONE* **9**, e96617.
- Fleagle JG.** (2013) Primate adaptation and evolution. 3rd ed. New York: Academic Press.
- Giavarina D.** (2015) Understanding Bland Altman analysis. *Biochem Med (Zagreb)* **25(2)**, 141-151.
- Gignac PM, Kley NJ.** (2014) Iodine-enhanced micro-CT imaging: Methodological refinements for the study of soft-tissue anatomy of post-embryonic vertebrates. *J Exp Zool B Mol Dev Evol* **322B**, 166-176.

- Gignac PM, Kley NK, Clarke JA, et al.** (2016) Diffusible iodine-based contrast-enhanced computed tomography (diceCT): an emerging tool for rapid, high-resolution, 3-D imaging of metazoan soft tissues. *J Anat* **228**, 889–909.
- Güngör E, Doğan MS.** (2017) Reliability and accuracy of cone-beam computed tomography voxel density and linear distance measurement at different voxel sizes: a study on sheep head cadaver. *J Dent Sci* **12**, 145-150.
- Hautier L, Lebrun R, Cox PG.** (2012) Patterns of covariation in the masticatory apparatus of hystricognathous rodents: implications for evolution and diversification. *J Morphol* **273**, 1319–1337.
- Herdina AN, Herzig-Straschil B, Hilgers H, et al.** (2010) Histomorphology of the penis bone (baculum) in the gray long-eared bat *Pleocotus austriacus* (Chiroptera, Vespertilionidae). *Anat Rec* **293**, 1248–1258.
- Herdina AN, Kelly DA, Jahelková H, et al.** (2015a) Testing hypotheses of bat baculum function with 3-D models derived from micro-CT. *J Anat* **226**, 229–235.
- Herdina AN, Plenk Jr. H, Benda P, et al.** (2015b) Correlative 3D-imaging of *Pipistrellus* penis micromorphology: Validating quantitative microCT images with undecalcified serial ground section histomorphology. *J Morphol* **276**, 695–706.
- Holliday CM, Tsai HP, Skiljan RJ, et al.** (2013) A 3-D interactive model and atlas of the jaw musculature of *Alligator mississippiensis*. *PLoS ONE* **8**, e62806.
- Hughes DF, Gignac PM, Walker EM, et al.** (2016) Rescuing perishable neuroanatomical information from a threatened biodiversity hotspot: Remote field methods for brain tissue preservation validated by semi-quantitative

cytoarchitectonic analysis, immunohistochemistry, and iodine-enhanced X-ray microcomputed tomography. *PLoS ONE* **11(5)**, e0155824.

Jeffrey NS, Stephenson RS, Gallagher JA, et al. (2011) Micro-computed tomography with iodine staining resolves the arrangement of muscle fibres. *J Biomech* **44**, 189-192.

Kupczik K, Stark H, Mundry R, et al. (2015) Reconstruction of muscle fascicle architecture from iodine-enhanced microCT images: A combined texture mapping and streamline approach. *J Theor Biol* **382**, 34-43.

Lagravere MO, Carey J, Toogood RW, et al. (2008) Three-dimensional accuracy of measurements made with software on cone-beam computed tomography images. *Am J Orthod Dentofacial Orthop* **134(1)**, 112-116.

Lautenschlager S, Bright JA, Rayfield EJ. (2013) Digital dissection—using contrast-enhanced computed tomography scanning to elucidate hard- and soft-tissue anatomy of the Common Buzzard *Buteo buteo*. *J Anat* **224**, 412–431.

Li Z, Ketcham RA, Yan F, et al. (2016) Comparison and evaluation of the effectiveness of two approaches of diffusible iodine-based contrast- enhanced computed tomography (diceCT) for avian cephalic material. *J Exp Zool B Mol Dev Evol* **00B**, 1–11.

Loubele M, Maes F, Schutyser F, et al. (2006) Assessment of bone segmentation quality of cone-beam CT versus multislice spiral CT: a pilot study. *Oral Surg Oral Med Oral Pathol Oral Radiol Endod* **102(2)**, 225-234.

Ludbrook J. (1997) Comparing methods of measurements. *Clin Exp Pharmacol Physiol* **24(2)**, 193-203.

- Metscher BD.** (2009a) Micro-CT for developmental biology: a versatile tool for high-contrast 3-D imaging at histological resolutions. *Dev Dyn* **238**, 632–640.
- Metscher BD.** (2009b) Micro-CT for comparative morphology: simple staining methods allow high-contrast 3D imaging of diverse non-mineralized animal tissues. *BMC Physiol* **9**, 11.
- Metscher BD.** (2013) Biological applications of X-ray microtomography: imaging micro-anatomy, molecular expression and organismal diversity. *Micros Anal* **27**, 13–16.
- Miller MN.** (1898) Students histology: a course of normal histology for students and practitioners of medicine. 3rd ed. New York: William Wood & Company.
- Mizutani R, Suzuki Y.** (2012) X-ray microtomography in biology. *Micron* **43**, 104-115.
- Moerenhout BA, Gelaude F, Swennen GRJ, et al.** (2009) Accuracy and repeatability of cone-beam computed tomography (CBCT) measurements used in the determination of facial indices in the laboratory setup. *J Craniomaxillofac Surg* **37**(1), 18-23.
- Neues F, Goerlich R, Renn J, et al.** (2007) Skeletal deformations in medaka (*Oryzias latipes*) visualized by synchrotron radiation micro-computer tomography (SRmicroCT). *J Struct Biol* **160**, 236-240.
- Pauwels E, Van Loo D, Cornillie P, et al.** (2013) An exploratory study of contrast agents for soft tissue visualization by means of high resolution X-ray computed tomography imaging. *J Microsc* **250**, 21-31.

- Periago DR, Scarfe WC, Moshiri M, et al.** (2008) Linear accuracy reliability of cone beam CT derive 3-dimensional images constructed using an orthodontic volumetric rendering program. *Angle Orthod* **78(3)**, 387-395.
- Peters OA, Laib A, Rügsegger P.** (2000) Three-dimensional analysis of root canal geometry by high-resolution computed tomography. *J Dent Res* **79(6)**, 1405-1409.
- Pinheiro HLN and Pontes ARM.** (2015) Home range, diet, and activity patterns of common marmosets (*Callithrix jacchus*) in very small and isolated fragments of the Atlantic forest of northeastern Brazil. *International Journal of Ecology* **2015** 685816.
- Ramírez MJ, Coddington JA, Maddison WP, et al.** (2007) Linking of Digital Images to Phylogenetic Data Matrices Using a Morphological Ontology. *Syst Biol* **56(2)**, 283-294.
- Rylands AB, Coimbra-Filho AF, Mittermeier RA.** (1993) Systematics, geographic distribution, and some notes on the conservation status of the Callitrichidae. In Rylands AB (ed), *Marmosets and tamarins: systematics, behaviour, and ecology*. Oxford University Press, Oxford, 11-77.
- Rylands AB, Mittermeier RA, de Oliveira MM, et al.** (2008) *Callithrix jacchus*. The IUCN Red List of Threatened Species **2008**: e.T41518A10485463.
- Sang Y-H, Hu H-C, Lu S-H, et al.** (2016) Accuracy assessment of three-dimensional surface reconstructions of in vivo teeth from cone-beam computed tomography. *Chin Med J (Engl)* **129(12)**, 1464-1470.
- Santana SE.** (2018) Comparative anatomy of bat jaw musculature via diffusible iodine-based contrast-enhanced computed tomography. *Anat Rec* **301**: 267-278.

- Seymour KL.** (1999) Taxonomy, morphology, paleontology and phylogeny of the South American small cats (Mammalia: Felidae). University of Toronto Ph.D. Thesis.
- Shaheen E, Khalil W, Ezeldeen M, et al.** (2017) Accuracy of segmentation of tooth structures using 3 different CBCT machines. *Oral Surg Oral Med Oral Pathol Oral Radiol* **123**(1), 123-128.
- Sombke A, Lipke E, Michalik P, et al.** (2015) Potential and limitations of X-Ray micro-computed tomography in arthropod neuroanatomy: A methodological and comparative survey. *J Comp Neurol* **523**, 1281-1295.
- Staedler YM, Masson D, Schönenberger J.** (2013) Plant tissues in 3D via x-ray tomography: Simple contrasting methods allow high resolution imaging. *PLoS ONE* **8**(9): e75295
- Stephenson RS, Boyett MR, Hart G, et al.** (2012) Contrast enhanced micro-computed tomography resolves the 3-dimensional morphology of the cardiac conduction system in mammalian hearts. *PLoS ONE* **7**(4), e35299.
- Tahara R, Larsson HCE.** (2013) Quantitative analysis of microscopic X-ray computed tomography imaging: Japanese quail embryonic soft tissues with iodine staining. *J Anat* **223**, 297-310.
- Tsai HP, Holliday CM.** (2011) Ontogeny of the alligator cartilage transiliens and its significance for sauropsid jaw muscle evolution. *PLoS ONE* **6**(9), e24935.
- Vasquez SX, Hansen MS, Bahadur AN, et al.** (2008) Optimization of volumetric computed tomography for skeletal analysis of model genetic organism *Anat Rec* **291**, 475-487.

- Vickerton P, Jarvis J, Jeffery N.** (2013) Concentration-dependent specimen shrinkage in iodine-enhanced microCT. *J Anat* **223**, 185-193.
- Vickerton P, Jarvis J, Gallagher JA, et al.** (2014) Morphological and histological adaptation of muscle and bone to loading induced by repetitive activation of muscle. *Proc Roy Soc B* **281**, 20140786.
- Whyms BJ, Vorperian HK, Gentry LR, et al.** (2013) The effect of CT scanner parameters and 3D volume rendering techniques on the accuracy of linear, angular, and volumetric measurements of the mandible. *Oral Surg Oral Med Oral Pathol Oral Radiol* **115(5)**, 682-691.
- Wong MD, Dorr AE, Walls JR, et al.** (2012) A novel 3-D mouse embryo atlas based on micro-CT. *Development* **129**, 3248–3256.
- Wong MD, Maezawa Y, Lerch JP, et al.** (2014) Automated pipeline for anatomical phenotyping of mouse embryos using micro-CT. *Development* **141**, 2533-2541.
- Wong MD, Spring S, Henkelman RM.** (2013) Structural stabilization of tissue for embryo phenotyping using micro-CT with iodine staining. *PLoS ONE* **8**, e84321.
- Yuen AHL, Tsui HCL, Kot BCW.** (2017) Accuracy and reliability of cetacean cranial measurements using computed tomography three dimensional volume rendered images. *PLoS ONE* **12(3)**, e0174215.
- Zimmermann D, Randolph S, Metscher BD, et al.** (2011) The function and phylogenetic implications of the tentorium in adult Neuroptera (Insecta). *Arthropod Struct Dev* **40**, 571-582.

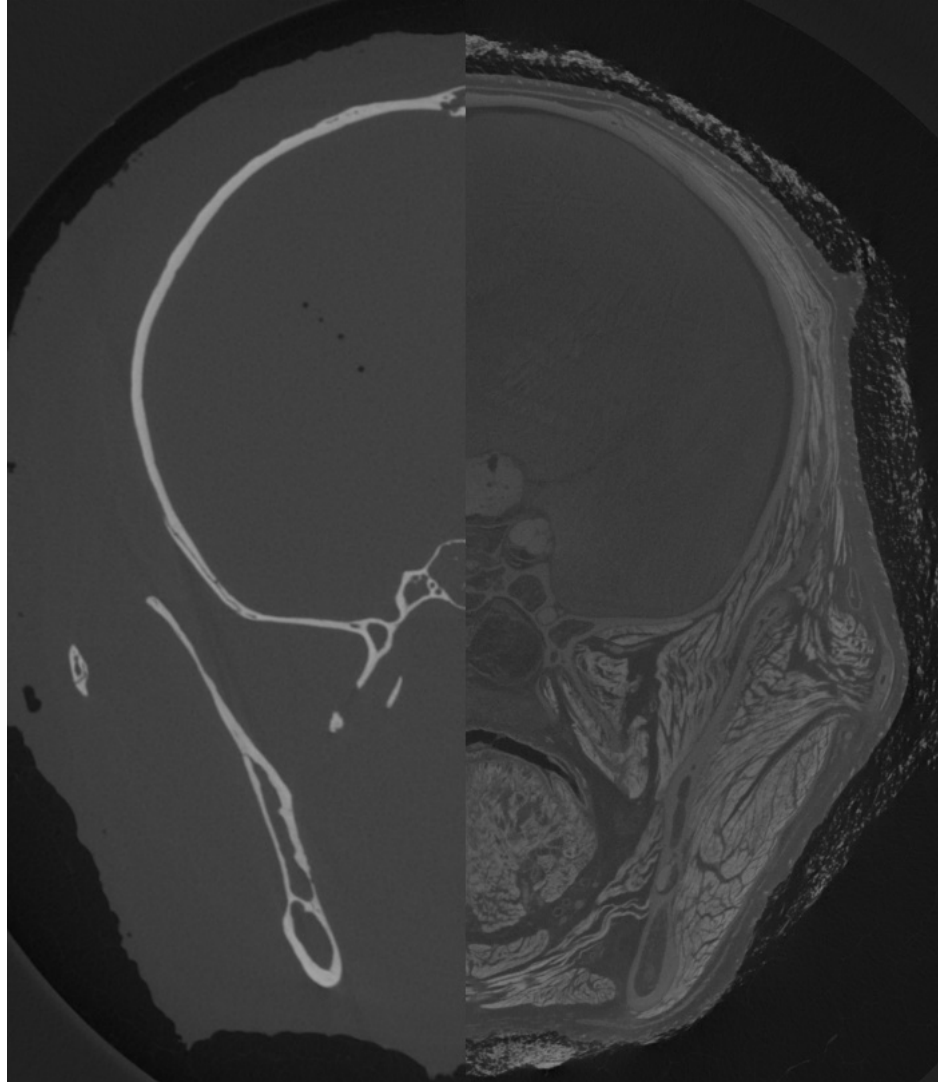


Figure 1. Side-by-side comparison of microCT (left) and diceCT (right) slices through the head of a *Callithrix jacchus*.

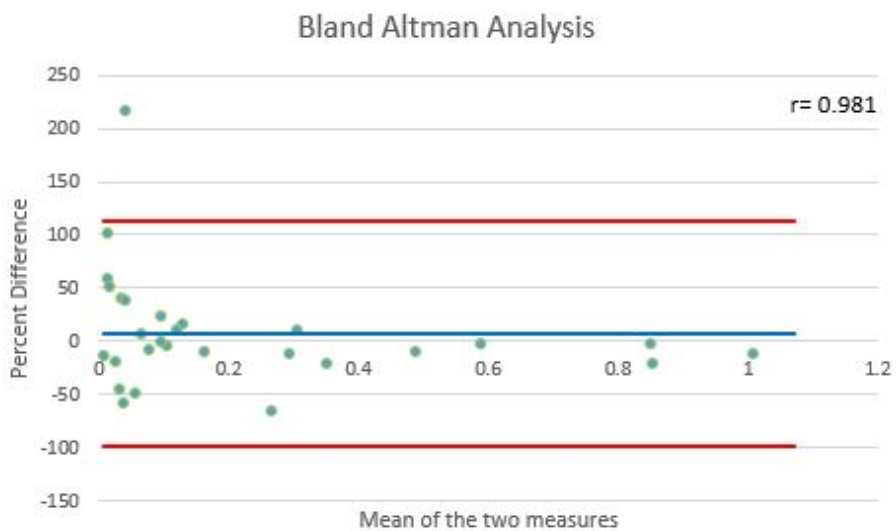


Figure 2. Bland Altman analysis of data from Bribiesca-Contreras & Sellers 2017. Using the data provided in Figure S2, a Bland-Altman analysis was produced with the blue line representing the mean line of equality (7.28%), calculated as the mean percent difference of all data pairs. The red lines are the 95% confidence intervals around the mean line of equality (-98.74%, 113.3%).

CHAPTER II

Analog vs digital: A comparative study between diceCT and gross dissection

This thesis follows the style and format of *Journal of Anatomy*.

Abstract

The use of diffusible iodine-based contrast-enhanced computed tomography (diceCT) has greatly expanded the use of computed tomography (CT) in recent years, revolutionizing the study of in situ soft tissues in three dimensions. This approach requires more research to compare measurements from CT and traditional dissection methods. To this end, the head of a common marmoset, *Callithrix jacchus*, was stained in 2.5% Lugol's solution for 37 days, with fresh solution supplied after 20 days, and studied digitally. Prior to staining, the head was CT scanned. Following staining, the head was CT scanned again, then physically dissected. Amira 5.6 was used to digitally segment and isolate soft tissue structures, comprising all four major tissue types: connective, epithelial, muscle, and nervous. Measurements were recorded to evaluate the difference between the digital and traditional dissections using multiple Bland-Altman analyses. Based on the analyses, gross dissection and diceCT are not interchangeable for all circumstances. Measurements were found to not be statistically similar in the case of connective tissue and linear measurements, but all other delineations of measurements were found to be significantly different between diceCT and gross dissection. This process is still widely beneficial when traditional destructive dissection is not possible. It allows for three dimensional views of structures that are not otherwise visible due to size and/or morphology, however, comparisons between gross dissection and diceCT should be approached with caution.

Keywords: Diffusible iodine-based contrast-enhanced computed tomography (diceCT), Gross dissection, Three-dimensional imaging, Comparison, *Callithrix jacchus*, Epithelial tissue, Muscle tissue, Volumetric data

Analog vs digital: A comparative study between diceCT and gross dissection

Introduction

Recently, researchers diffusible iodine-based contrast-enhanced computed tomography (“diceCT”) (sensu Gignac et al. 2016) have generated biomechanical models for investigating a variety of medical, functional morphological, and phylogenetic questions (Metscher, 2009a,b; Cox et al. 2011, 2012; Cox & Jeffery, 2011; Baverstock et al. 2013; Cox & Faulkes, 2014; Vickerton et al. 2014; Herdina et al. 2015a; Clarke et al. 2016). As diceCT is proposed as a dissection alternative (Gignac et al. 2016), it must be tested against traditional gross dissection methods to evaluate equivalency in measurements generated. Here I will test how the data produced using diceCT compares to the data produced by traditional gross dissection, to assess the comparability of the two methods.

History of Computed Tomography. Computed tomography (CT) is increasingly used in biology and medical sciences, with microCT, a higher resolution of computed tomography, first utilized to analyze mineralized tissues (Elliot and Dover, 1982). Recently a variation of the method was introduced to analyze soft tissue (Metscher, 2009a,b). Since microCT does not distinguish soft tissue, a contrast agent is needed to enhance visualization of less radiopaque materials (Metscher, 2009a,b). When compared, the distinction between diceCT and microCT is apparent (*Figure 1*).

Several staining radiopaque compounds are used to enhance the contrast on CT scans, with iodine based methods, such as iodine in ethanol (e.g. Metscher, 2009a,b; Herdina et al. 2010, 2015a,b; Clarke et al. 2016), and Lugol’s iodine (e.g. Metscher, 2009a,b; Cox & Jeffery, 2011; Holliday et al. 2013; Gignac et al. 2016; Santana, 2018),

being the primary reagents used among current researchers (Gignac et al. 2016). DiceCT has been used to visualize organisms across many taxa, such as alligators (Holliday et al. 2013), bats (Santana, 2018), and centipedes (Sombke et al. 2015), making it a valuable tool to many researchers. The staining process can reveal all four types of tissue; connective, epithelial, muscular, and nervous (Gignac et al. 2016).

Assumption of Comparability.

Traditional CT Comparability. Traditional CT produces statistically comparable linear (Loubele et al. 2006; Lagravere et al. 2008; Periago et al. 2008; Brown et al. 2009; Moerenhout et al. 2009; Damstra et al. 2010; Güngör & Doğan, 2017; Yuen et al, 2017) and volumetric measurements (Albuquerque et al. 2011; Whyms et al. 2013; Sang et al. 2016; Shaheen et al. 2017) for bone. However, these findings do not necessarily apply to diceCT, because the presence of soft tissue in scans may affect both linear and volumetric measurements of bone in CT (Dusseldorp et al. 2017). Those differences in linear and volumetric measurements may be more pronounced when using diceCT, because bone decreases in contrast when stained in Lugol's iodine (Metscher, 2009a; Cox & Jeffery, 2011; Baverstock et al. 2013; Gignac & Kley, 2014).

Inadequate Comparisons. Comparisons between diceCT and gross dissection do not show enough statistical support to be the sole support of the proposition that these methods are equivalent. Histological methods have been used for direct comparison to diceCT and deemed to be correlated, but no measurements or statistical analysis between the datasets were reported (Jeffery et al. 2011; Stephenson et al. 2012; Herdina et al. 2015b). Histology has also been used as an indirect, qualitative, comparison to diceCT, meaning different specimens from those that underwent diceCT were histologically

prepared (Degenhardt et al. 2010; Herdina et al. 2010; Tsai & Holliday, 2011; Taraha & Larsson, 2013; Wong et al. 2013; Vickerton et al. 2014). A one-to-one comparison would be the best means for determining equivalency, but so far studies have been limited due to sample size, use of averages, and/or lack of statistics (Degenhardt et al. 2010; Herdina et al. 2010; Baverstock et al. 2013; Kupczik et al. 2015). An average cannot be a true one-to-one comparison of the measurements. A one-to-one comparison is necessary to ensure that the same structures are measured, removing a degree of uncertainty from the statistical analysis.

Only three performed true one-to-one comparisons, measuring the same structures in both diceCT and traditional gross dissection studies (Vickerton et al. 2013; Bribiesca-Contreras & Sellers, 2017; Santana, 2018). Traditional gross dissection and diceCT were found to produce significantly different physiological cross-sectional areas (Santana, 2018). Other studies argue that there is not a significant difference between the two methods, but this was established by means of a linear regression (Vickerton et al. 2013; Bribiesca-Contreras & Sellers, 2017). A linear regression is considered an inappropriate standard by which to compare two methods, as regressions are meant to study cause and effect, not the differences between two sets of data (Ludbrook, 1997; Giavarina, 2015), with a Bland-Altman analysis preferred (Altman and Bland, 1983).

Impact. The lack of comparative studies between gross dissection and diceCT is problematic; for example, many studies (e.g. Herdina et al. 2010; Stephenson et al. 2012; Wong et al. 2012, 2013; Vickerton et al. 2014; Sombke et al. 2015) compare quantitative data to the literature using potentially inequivalent or incomparable data, which could lead to misinformed conclusions if the methods are not comparable. Those comparisons

of quantitative data to the literature are made with both traditional gross dissection measurements (e.g. Kupczik et al. 2015) and diceCT measurements (e.g. Cox & Faulkes, 2014 compared to Cox & Jeffery, 2011), making it more difficult to assess the validity of conclusions. Linear and volumetric data from traditional gross dissection may not be comparable to diceCT, necessitating the testing of diceCT and traditional gross dissection. Mixed data methods (i.e. when authors use multiple methods to complement one another) assume equivalency, though the two methods have not been shown to be equivalent.

Many studies include scale bars on digital models, without explicit comparison statistics or any support to their validity (e.g. Degenhardt et al, 2010; Herdina et al. 2010, 2015a,b; Hautier et al, 2012; Sombke et al. 2015). When physical specimens cannot be obtained it is common to use specimen images to generate characters for phylogenetic analysis (e.g. Seymour, 1999; Ramírez et al. 2007). 3D pdfs that allow for direct interaction and measurements of specimens have been published, in part, with these goals in mind (Düring et al. 2013; Holliday et al. 2013; Lautenschlager et al. 2013; Cox & Faulkes, 2014; Herdina et al. 2015a; Sombke et al. 2015; Clarke et al. 2016). Unfortunately, some do not activate properly to allow interaction (Clarke et al, 2016), some no specified units (Düring et al. 2013; Sombke et al. 2015), and some are not properly calibrated (Düring et al. 2013; Lautenschlager et al. 2013; Herdina et al. 2015a), resulting in inflated measurements. These 3D pdfs have to be calibrated by the original author, otherwise these errors will occur. They can be corrected by redefining the model units, which are not typically provided. In those cases, there was an error and the 3D pdf needs to be recalibrated, but it may not always be evident that a mistake has been made.

If the digital model measurements prove to be incomparable to gross dissection, the resultant models, which are typically based off gross dissection, may be compromised, ultimately affecting the conclusions drawn.

Lack of Physical Dissection. In many projects utilizing diceCT, no physical dissections were performed to be used for direct comparison to diceCT methods (e.g. Tsai & Holliday, 2011; Wong et al. 2012, 2013, 2014; Düring et al. 2013; Anderson & Maga, 2015). While the difficulty of measuring exceedingly small objects in dissection as support for using diceCT is occasionally discussed (e.g. Cox & Jeffery, 2011; Stephenson et al. 2012; Baverstock et al. 2013; Lautenschlager et al. 2013; Herdina et al. 2015b), without physical dissections, diceCT cannot be evaluated for comparison with gross dissection.

After reviewing the literature, it becomes apparent that a comparative study between the traditional gross dissection and digital dissection based on diceCT would yield valuable information about the comparability and compatibility of these methods. I hypothesize that measurements obtained from gross dissection and diceCT on a *Callithrix jacchus* specimen will not be significantly different. This hypothesis is being tested as it is the working assumption that previous researchers in the field have used. It is imperative to test this assertion to ensure that previous works can be reinforced, and future work can be performed in confidence.

Methods

Staining. A common marmoset, *Callithrix jacchus*, was chosen due to its size allowing for both scanning and dissection, as well as its use in another study. Due to the propensity of diceCT research revolving around the head, it was selected to study. The

use of the common marmoset head also appeals to physical anthropology researchers, as there is a focus on the skull and masticatory muscles. The common marmoset died in captivity, before being frozen. The head was removed from the frozen individual (*Figure 3*), so no Institutional Animal Care and Use Committee approval was necessary.

The head was fixed in 10% formalin prior to staining, and soaked in 2.5% I₂KI (Lugol's solution) in multiple stages over several weeks for improved contrast (Jeffrey et al. 2011; Li et al. 2015; Kupczik et al. 2015; Gignac et al. 2016). Lugol's iodine was chosen over other staining techniques, because it improves visualization of muscle fibers, especially relative to iodine in ethanol (Li et al. 2016), which are important for future analyses with this specimen. The concentration selected was chosen with the intent of minimizing tissue shrinkage, because shrinkage dramatically increases with higher concentrations of Lugol's solution (Vickerton et al, 2013). The staining solution was replaced to keep the specimen in fresh Lugol's solution after 20 days, and the specimen kept in solution until experts at the scanning facility believed it would produce the highest quality images for analysis, which totaled 37 days.

Scanning. Scanning was performed at The University of Texas High-Resolution X-ray Computed Tomography Facility (UTCT) on a North Star Imaging (NSI) scanner, using the ultra-high-resolution subsystem. An initial scan, prior to iodine staining, at 150kV, 0.1 mA, and voxel size 45.4 μm (e.g. Gignac et al. 2016) was performed for bone comparison sub-hypotheses, as bone shows up best prior to staining procedures (Baverstock et al. 2013; Gignac et al. 2016; Li et al. 2016). During staining, test scans were performed every two days to ensure that the specimen was not oversaturated (Gignac et al. 2016). A final scan, once appropriately saturated, was performed at 150kV,

0.14mA, and voxel size 25.6 μ m (following Gignac et al. 2016; Table 1). Difference in voxel size is seen to be insignificant to volumetric reconstructions when voxel size is kept at or below 76 μ m (Damstra et al. 2010; Maret et al. 2012, 2014; Sang et al. 2016). Both scans produced 16-bit TIFF and 8-bit JPEG image files of the slices.

Segmentation. Both 16-bit and 8-bit datasets were produced, with the 8-bit being used based on computational power and the advice from the UTCT operators. Using the 8-bit JPEG image files, structures were digitally segmented and rendered to be measured. These structures were chosen so the study would have a wide sample of tissues and tissue types for analysis, as well as the feasibility of removing the structures without damage. Segmentation is the selection of pixels from each slice of the scan to be reconstructed into a three-dimensional model (*Figure 4*). Segmentation was performed using Amira 5.6; specifically, the segmentation editor and the suite of tools available within, including the paintbrush, magic wand, and threshold tools. The paintbrush tool allowed for manual coloring of pixels to be assigned to a specific material. The magic wand used differences in greyscale values to approximate borders between structures, and the threshold tool allowed for the selection of only those pixels that fell in the desired range of greyscale values. Automatic thresholding and segmenting procedures were not used as they are known to cause false-positive and false-negative voxels to be segmented (Wong et al. 2012; Balanoff et al. 2015). A false-positive voxel would be one that has been segmented as a certain material when it is not part of that material, while a false-negative voxel would be one that should be segmented as a particular material but has not been segmented as that material, if at all.

Rendering. Volume Rendering, for viewing segmented structures and obtaining images, was performed in Amira 5.6 using the surface generator and isosurface tools without any smoothing effects outside of the default programming (*Figure 4*).

Measurements were taken using the material statistics function for volumes (Appendix, and the 3D length tool for one-dimensional measurements such as lengths, widths, and heights. Images of renders were captured using the snapshot tool, in order to create figures.

Gross Dissection. Dissection of structures of interest was performed at the University of South Carolina by a researcher, Carissa Leischner, with experience dissecting primates to ensure accurate identifications and procedures (Hartstone-Rose et al. 2018; Leischner et al. 2018). First, the skin was removed and measured (*Figure 5*), then the most external structures were removed (e.g. parotid gland, superficial masseter, deep masseter, etc.) followed by progressively more internal structures (e.g. temporalis, medial pterygoid, lateral pterygoid, etc.) until all structures of interest were removed. This took place first on the right side of the head, then the left, resulting in the mandible being detached from the rest of the skull. Digital calipers were used on the clean skull to measure distances (e.g. Damstra et al. 2010; Whyms et al. 2014; Sang et al. 2016).

Archimedes Method. The Archimedes method was used to measure volumes of irregular solids (Table 2), a technique used in previous studies (Whyms et al. 2013; Sang et al. 2016; Shaheen et al. 2017). The Archimedes method is based on volume displacement, having the irregular solid whose volume is unknown placed into a previously measured amount of liquid. The change in volume is equal to the volume of the solid dropped in. This was done using graduated cylinders and measuring the water

levels before and after the addition of the object, allowing time for any air bubbles to be eliminated.

Specific Muscle Density Method. The specific density of muscle, 1.0564 g/cm^3 (Murphy and Beardsley, 1974), was used to convert gross dissection masses to volumes (Table 2), similar to other studies (Baverstock et al. 2013; Cox & Faulkes, 2014).

Statistical Analysis. Bland-Altman analysis was used to compare the diceCT and traditional gross dissection for all linear and volumetric measurements (Altman and Bland, 1983; Ludbrook, 1997; Critchley & Critchley, 1999; Giavarina, 2015). The analysis was performed for the whole dataset, linear (1D) measurements only, volumetric (3D) measurements only, connective tissue only, muscular tissue only, epithelial tissue only, and nervous tissue only. Correlations are not solely reliable in method comparisons (Altman and Bland, 1983; *Figure 6*), as they can be easily influenced by a single data point (Anscombe, 1973). Therefore, the Altman and Bland method of analyses (1983) was performed, calculating the mean bias of the differences between the two measurements as a way to analyze precision. Those differences are then plotted against the average for each pair, while limits of agreement and 95% confidence intervals around the mean bias are also calculated (Altman and Bland, 1983). Bland and Altman plot analysis generates a mean line of equality within the lines of agreement (Giavarina, 2015). Bland and Altman (1983) originally suggested using the true difference, but for studies like this one, where there is a large range of measurements, Critchley & Critchley (1999) suggest using percent difference instead, because this will eliminate bias due to magnitude of the measurements. For the purposes of this study, the percent difference allowed by the Bland-Altman analysis was restricted to $\pm 30\%$ for the 95% confidence

intervals for diceCT to be considered comparable to traditional gross dissection, a standard set forth previously (Critchley & Critchley, 1999).

Results

The data obtained from the digital and gross dissections was used as one dataset, and broken down by subset to address the hypotheses. A Bland-Altman analysis performed using all the data shows a significant difference between the two methods (*Figure 7*). Digital measurements from diceCT ($n=37$; $r=0.965$) were 10.84% larger than those obtained via traditional gross dissection. The lines of agreement were found to be at +92.09% and -70.42%, outside of the significance threshold set forth previously (Critchley & Critchley, 1999).

Connective. Measurements for connective tissue ($n=13$; $r=1.000$) were insignificantly different, with lines of agreement at +17.67% and -21.95% (*Figure 8*). Digital diceCT measurements were found to be 2.14% smaller than traditional gross dissection measurements on average. Much of the connective tissue, excluding bone, was found to be tough and hard.

The bone of the specimen was found to be more flexible and pliable during gross dissection following staining. The grayscale values of the voxels for the stained and unstained mandible changed considerably when comparing the unstained mandible to the stained (Table 3). The distribution of the grayscale values also changed (*Figure 9*).

Epithelial. Measurements of epithelial tissue ($n=5$; $r=0.723$) were on average 42.90% larger in diceCT than the measurements from gross dissection (*Figure 10*). This placed lines of agreement at +204.35% and -118.55%, indicating a significant difference.

The right lens was unable to be found, as the eye lost much of its structural integrity after staining.

Nervous. Gross dissection measurements from nervous tissue were only successful for the spinal cord diameter. Since the Bland-Altman analysis requires a minimum of two points to use, only a percent difference could be calculated, with diceCT yielding a 2.07% longer measurement than gross dissection. The optic nerve was observed to be much harder than normal, similar to plastic, and appeared more fibrous. The optic nerve was unable to be removed without damage.

Muscle. Measurements from gross dissection and diceCT for all musculature were used in a Bland-Altman analysis ($n=18$; $r=0.979$), yielding a mean 9.42% difference, and with lines of agreement at +93.63% and -74.80% (*Figure 11*).

During the gross dissection, the right temporalis was unable to be separated into the deep and superficial portions, so results were obtained for the whole temporalis instead. During digital dissection, difficulties arose in identifying the border between adjacent muscles, such as the superficial and deep masseters. When this occurred, best judgement was used to decide where the border lay. This was a concern on the superior half of the deep and superficial temporalis muscles, and the anterior portion of the deep and superficial masseter muscles. Difficulty was also posed by the inferior part of the zygomatic temporalis, where it came into contact with the zygomatico-mandibularis.

Mastication muscles were broken down in terms of volume, percent of overall volume for each side of the specimen, and when applicable, the percentage that each constituent part of a muscle makes up of the larger structure (Table 4).

Linear. Bland-Altman analysis for all linear measurements ($n=15$; $r=0.996$) taken during both the gross dissection and the digital dissection are shown to be within the $\pm 30\%$ threshold ($+24.63\%$, -19.90%) and are not significantly different, with a 2.37% difference (*Figure 12*).

Volumetric. Volumetric data was taken from the mandible, as well as several glands and muscles (*Figure 13*). Volumetric measurements ($n=22$; $r=0.957$) in gross and digital dissection yielded significantly different results, looking at the lines of agreement of the Bland-Altman analysis ($+119.843\%$, -86.62% , *Figure 14*). On average, the two methods differed by 16.61%.

The Archimedes method and the specific muscle density method were each used to measure about half of the volumetric data. The Archimedes' method ($n=12$; $r=0.95$) yielded diceCT values that were 3.59% larger than gross dissection methods. Lines of agreement were found to be at $+119.62\%$ and -112.43% (*Figure 15*).

The specific muscle density method, using the constant of 1.0564 g/cm^3 (Murphy and Beardsley, 1974) constitutes the rest of the volumetric data ($n=10$; $r=0.948$) and yielded diceCT values that were 32.24% larger than gross dissection methods. Lines of agreement were found to be at $+112.87\%$ and -48.40% . (*Figure 16*). The data from the Archimedes' method and the specific muscle density method are independent of each other.

Discussion

Prior to this study, it was not understood how diceCT measurements compared to their gross dissection counterparts. DiceCT is already being used for measurements (e.g. Cox & Jeffery, 2011; Baverstock et al. 2013; Holliday et al. 2013; Bribiesca-Contreras &

Sellers, 2017) and subsequent models (Cox et al. 2012; Vickerton et al. 2014). Data collected from connective, epithelial, muscle, and nervous tissue indicates that measurements from diceCT and traditional gross dissection are significantly different and should not, therefore, be used interchangeably.

Tissue Type. Analyzing the results by tissue type, both epithelial and muscle tissue are significantly different between diceCT and gross dissection. This difference between diceCT and gross dissection volume measurements could partly be due to muscle shrinkage. It has been demonstrated that *ex vivo* muscles stained in 2% I₂KI dissolved in 10% formalin caused an average loss of 26% volume after two weeks (Vickerton et al. 2013). While this is a larger difference than the average seen in this work, shrinkage is suggested to be less severe *in situ*, because muscles are still attached to support structures (i.e. bones and cartilage) (Vickerton et al. 2013). Buytaert et al. (2014) observed 42% volume loss in muscles using a 3% I₂KI solution. Nearly half (18/37 or 48.6%) of the results of this study are derived from muscle tissue, skewing the overall finding strongly towards the gross dissection and diceCT being incompatible.

Epithelial tissue comparisons were not previously reported, but the significantly different results presented here suggest the right parotid gland and right submandibular gland were 111% and 133% larger in diceCT than in gross dissection. The glands show considerable interstitial space in the diceCT slices, which would increase the volume considerably if it were not accounted for in gross dissection. Interstitial spaces would allow water from the Archimedes method to fill in glands, negating interstitial space in Archimedes method measurements, and yielding much smaller volumes using the Archimedes method. There could also be an interaction between the staining mechanism

(Lugol's iodine) and the glands that cause them to swell. This effect may then dissipate when glands are placed in water for displacement measurement. This issue needs further study to better clarify these results.

Connective tissue was found to be statistically similar between diceCT and gross dissection, but given the other significant differences presented here, comparisons involving diceCT and gross dissection measurements should be approached with caution. Nervous tissue was degraded by the iodine, possibly due to shrinkage, causing the tissue to become brittle and dense.

Linear and Volumetric. Results were also analyzed by delineating between linear and volumetric measurements. Linear results show diceCT to be statistically similar to gross dissection. Conversely, volumetric measurements were found to be significantly different in diceCT as compared to traditional gross dissection.

When the volumetric data from this study is further broken down into the two methods used for retrieval (i.e. Archimedes method and specific muscle density method), both yield significantly different numbers from diceCT. For the Archimedes method, only two (right submandibular gland, right parotid gland) out of 12 measurements were found to have a difference greater than 50%. Three (left zygomatic temporalis, left deep masseter, and left medial pterygoid) out of ten measurements using the specific muscle density method were found to be more than 50% different. These differences may be attributed to the same issues regarding shrinkage and methodology for epithelial and muscle tissue mentioned previously. Issues with differences in volumetric measurements, especially using the Archimedes method are likely due to the difficulty with measuring small volumes using traditional gross dissection.

DiceCT Accuracy. This study cannot and does not suggest one method is more accurate than another, but it does show that there is a significant difference between volumetric measurements in diceCT and traditional gross dissection. DiceCT has some advantages over dissection in that it is non-destructive, can be corrected if errors are detected in segmentation, and it allows the ability to view *in situ* structures in 3D.

Limitations. A potential source of error for this study comes from the difficulty in identifying the boundaries of muscles, especially those that are part of the same larger structure (e.g., superficial vs deep masseter; superficial vs deep temporalis). For instance, the left masseter as a whole is very similar between the two methods, but the left deep masseter and the left superficial masseter are not (Table 4). The deep masseter is about 28 mm³ larger in diceCT than in traditional dissection, while the superficial masseter is about 22 mm³ smaller in diceCT than in traditional dissection. These differences may be caused by misidentification of the division between the deep and superficial masseter, leading to superficial masseter being misattributed to deep masseter.

Sample size is a concern moving forward. More samples, particularly for volumetric connective tissue, linear and volumetric epithelial tissue, linear muscle tissue, and linear and volumetric nervous tissue measurements would improve analysis. More measurements were originally planned, but the iodine staining that took place for this study damaged nervous and connective tissue. The small size of the specimen, while ideal for staining and scanning, provided samples that were difficult to measure using traditional gross dissection, suggesting that a larger specimen may be better for this type of study. Additionally, using the whole body would provide more opportunity to obtain samples of all tissue types, including cardiac muscle tissue. Measurements also need to

be performed for volumetric muscle tissue using both Archimedes and specific muscle density measurements for the same muscles, an oversight that was made in this study, preventing comparison of the two methods. Given the lack of sample size in the previously mentioned areas, the findings of this study are most strongly supported for linear connective tissue measurements and volumetric muscle measurements.

Conclusions

Based on the results, future work needs focus on epithelial and nervous tissue. Both tissue types need better comparisons to see if the diceCT and traditional gross dissection are compatible for each tissue type. More work also needs to be done to understand if there is a difference between the Archimedes method and specific muscle density method. Further study will provide a clearer understanding of the relationship between the two methods. The reason for the significant difference between diceCT and traditional gross dissection needs to be further evaluated to better understand the roles diceCT and gross dissection should play in anatomical research.

It may be concluded that diceCT results are not interchangeable with traditional gross dissection, and should not be used as such. This study will serve to prevent the erroneous comparing of diceCT and traditional gross dissection data. This will prevent mixed models and other comparisons from making flawed conclusions, in turn improving models and better answering anatomical questions.

Acknowledgements

I thank PJ Lewis, A Hartstone-Rose, JD Daza, and JK Williams for their feedback and assistance on this manuscript. Additionally, I thank CL Leischner, JA Costa, L Rudie, C Fakhri, S Mesa, and C Basham for data acquisition assistance, The University

of Texas CT Lab for scanning support, and KM Jenkins for edits and discussions. This work was supported, in part, by the National Science Foundation (NSF IOS-15-57125).

References

- Albuquerque MA, Gaia BF, Cavalcanti MG.** (2011) Comparison between multislice and cone-beam computerized tomography in the volumetric assessment of cleft palate. *Oral Surg Oral Med Oral Pathol Oral Radiol Endod* **112(2)**, 249-257.
- Altman DG, Bland JM.** (1983) Measurement in medicine: The analysis of method comparison studies. *J R Stat Soc* **32**, 307-317.
- Anderson R, Maga AM.** (2015) A novel procedure for rapid imaging of adult mouse brains with microCT using iodine-based contrast. *PLoS ONE* **10(11)**: e0142974.
- Anscombe FJ.** (1973) Graphs in statistical analysis. *The American Statistician* **27**, 17–21.
- Balanoff AM, Bever GS, Colbert MW, et al.** (2015) Best practices for digitally constructing endocranial casts: examples from birds and their dinosaurian cousins. *J Anat* **229**, 173-190.
- Baverstock H, Jeffery NS, Cobb SN** (2013) The morphology of the mouse masticatory musculature. *J Anat* **223**, 46–60.
- Bribiesca-Contreras F, Sellers WI.** (2017) Three-dimensional visualization of the internal anatomy of the sparrowhawk (*Accipiter nisus*) forelimb using contrast-enhanced micro-computed tomography. *PeerJ* **5**: e3039.
- Brown AA, Scarfe WC, Scheetz JP, et al.** (2009) Linear accuracy of cone beam CT derived 3D images. *Angle Orthod* **79(1)**, 150-157.

- Buytaert J, Goyens J, De Greef D, et al.** (2014) Volume shrinkage of bone, brain, and muscle tissue in sample preparation for micro-CT and light sheet fluorescence microscopy (LSFM). *Microsc Microanal* **20**, 1208-1217.
- Clarke JA, Chatterjee S, Li Z, et al.** (2016) Fossil evidence of the avian vocal organ from the Mesozoic. *Nature* **538**, 502–505
- Cox PG, Fagan MJ, Rayfield EJ, et al.** (2011) Finite element modeling of squirrel, guinea pig and rat skulls: using geometric morphometrics to assess sensitivity. *J Anat* **219**, 696–709.
- Cox PG, Faulkes CG.** (2014) Digital dissection of the masticatory muscles of the naked mole-rat, *Heterocephalus glaber* (Mammalia, Rodentia). *PeerJ* **2**, e448.
- Cox PG, Jeffery N.** (2011) Reviewing the morphology of the jaw-closing musculature in squirrels, rats, and guinea pigs with contrast-enhanced micro-CT. *Anat Rec* **294**, 915–928.
- Cox PG, Rayfield EJ, Fagan MJ, et al.** (2012) Functional evolution of the feeding system in rodents. *PLoS ONE* **7**, e36299.
- Critchley LAH, Critchley AJH.** (1999) A meta-analysis of studies using bias and precision statistics to compare cardiac output measurement techniques. *J Clin Monit Comput* **15(2)**, 85-91.
- Damstra J, Fourie Z, Huddleston Slater JJR, et al.** (2010) Accuracy of linear measurements from cone-beam computed tomography-derived surface models of different voxel sizes. *Am J Orthod Dentofacial Orthop* **137**, 16.e1-16.e6.

- Degenhardt K, Wright AC, Horng D, et al.** (2010) Rapid 3D phenotyping of cardiovascular development in mouse embryos by micro-CT with iodine staining. *Circ Cardiovasc Imaging* **2010(3)**, 314-322.
- Düring DN, Ziegler A, Thompson CK, et al.** (2013) The songbird syrinx morphome: a three-dimensional, high-resolution, interactive morphological map of the zebra finch vocal organ. *BMC Biol* **11**, 1.
- Dusseldorp JK, Stamatakis HC, Ren Y.** (2017) Soft tissue coverage on the segmentation accuracy of the 3D surface-rendered model from cone-beam CT. *Clin Oral Invest* **21**, 921-930.
- Elliot JC, Dover SD.** (1982) X-ray microtomography. *J Microsc* **126(2)**, 211-213.
- Giavarina D.** (2015) Understanding Bland Altman analysis. *Biochem Med (Zagreb)* **25(2)**, 141-151.
- Gignac PM, Kley NJ.** (2014) Iodine-enhanced micro-CT imaging: Methodological refinements for the study of soft-tissue anatomy of post-embryonic vertebrates. *J Exp Zool B Mol Dev Evol* **322B**, 166-176.
- Gignac PM, Kley NK, Clarke JA, et al.** (2016) Diffusible iodine-based contrast-enhanced computed tomography (diceCT): an emerging tool for rapid, high-resolution, 3-D imaging of metazoan soft tissues. *J Anat* **228**, 889–909.
- Güngör E, Doğan MS.** (2017) Reliability and accuracy of cone-beam computed tomography voxel density and linear distance measurement at different voxel sizes: a study on sheep head cadaver. *J Dent Sci* **12**, 145-150.
- Hartstone-Rose A, Deutsch AR, Leischner CL, et al.** (2018) Dietary correlates of primate masticatory muscle fiber architecture. *Anat Rec* **301(2)**, 311-324.

- Hautier L, Lebrun R, Cox PG.** (2012) Patterns of covariation in the masticatory apparatus of hystricognathous rodents: implications for evolution and diversification. *J Morphol* **273**, 1319–1337.
- Herdina AN, Herzig-Straschil B, Hilgers H, et al.** (2010) Histomorphology of the penis bone (baculum) in the gray long-eared bat *Pleocotus austriacus* (Chiroptera, Vespertilionidae). *Anat Rec* **293**, 1248–1258.
- Herdina AN, Kelly DA, Jahelková H, et al.** (2015a) Testing hypotheses of bat baculum function with 3-D models derived from micro-CT. *J Anat* **226**, 229–235.
- Herdina AN, Plenk Jr. H, Benda P, et al.** (2015b) Correlative 3D-imaging of *Pipistrellus* penis micromorphology: Validating quantitative microCT images with undecalcified serial ground section histomorphology. *J Morphol* **276**, 695–706.
- Holliday CM, Tsai HP, Skiljan RJ, et al.** (2013) A 3-D interactive model and atlas of the jaw musculature of *Alligator mississippiensis*. *PLoS ONE* **8**, e62806.
- Jeffrey NS, Stephenson RS, Gallagher JA, et al.** (2011) Micro-computed tomography with iodine staining resolves the arrangement of muscle fibres. *J Biomech* **44**, 189-192.
- Kupczik K, Stark H, Mundry R, et al.** (2015) Reconstruction of muscle fascicle architecture from iodine-enhanced microCT images: A combined texture mapping and streamline approach. *J Theor Biol* **382**, 34-43.
- Lagravere MO, Carey J, Toogood RW, et al.** (2008) Three-dimensional accuracy of measurements made with software on cone-beam computed tomography images. *Am J Orthod Dentofacial Orthop* **134(1)**, 112-116.

- Lautenschlager S, Bright JA, Rayfield EJ.** (2013) Digital dissection—using contrast-enhanced computed tomography scanning to elucidate hard- and soft-tissue anatomy of the Common Buzzard *Buteo buteo*. *J Anat* **224**, 412–431.
- Leischner CL, Crouch M, Allen KL, et al.** (2018) Scaling of primate forearm muscle architecture as it relates to locomotion and posture. *Anat Rec* **301(3)**, 484-495.
- Li Z, Clarke JA, Ketcham RA, et al.** (2015) An investigation of the efficacy and mechanism of contrast-enhanced x-ray computed tomography utilizing iodine for large specimens through experimental and simulation approaches. *BMC Physiol* **15**, 5, 16pp.
- Li Z, Ketcham RA, Yan F, et al.** (2016) Comparison and evaluation of the effectiveness of two approaches of diffusible iodine-based contrast- enhanced computed tomography (diceCT) for avian cephalic material. *J Exp Zool B Mol Dev Evol* **00B**, 1–11.
- Loubele M, Maes F, Schutyser F, et al.** (2006) Assessment of bone segmentation quality of cone-beam CT versus multislice spiral CT: a pilot study. *Oral Surg Oral Med Oral Pathol Oral Radiol Endod* **102(2)**, 225-234.
- Ludbrook J.** (1997) Comparing methods of measurements. *Clin Exp Pharmacol Physiol* **24(2)**, 193-203.
- Maret D, Peters OA, Galibourg A, et al.** (2014) Comparison of the accuracy of 3-dimensional cone-beam computed tomography and micro-computed tomography reconstructions by using different voxel sizes. *J Endod* **39**, 394-397.
- Maret D, Telmon N, Peters OA, et al.** (2012) Effect of voxel size on the accuracy of 3D reconstructions with cone beam CT. *Dentomaxillofac Radiol* **41**, 649-655.

- Metscher BD.** (2009a) Micro-CT for developmental biology: a versatile tool for high-contrast 3-D imaging at histological resolutions. *Dev Dyn* **238**, 632–640.
- Metscher BD.** (2009b) Micro-CT for comparative morphology: simple staining methods allow high-contrast 3D imaging of diverse non-mineralized animal tissues. *BMC Physiol* **9**, 11.
- Metscher BD.** (2013) Biological applications of X-ray microtomography: imaging micro-anatomy, molecular expression and organismal diversity. *Micros Anal* **27**, 13–16.
- Moerenhout BA, Gelaude F, Swennen GRJ, et al.** (2009) Accuracy and repeatability of cone-beam computed tomography (CBCT) measurements used in the determination of facial indices in the laboratory setup. *J Craniomaxillofac Surg* **37**(1), 18-23.
- Murphy RA, Beardsley AC.** (1974) Mechanical properties of the cat soleus muscle in situ. *Am J Physiol* **227**(5), 1008-1013
- Periago DR, Scarfe WC, Moshiri M, et al.** (2008) Linear accuracy reliability of cone beam CT derive 3-dimensional images constructed using an orthodontic volumetric rendering program. *Angle Orthod* **78**(3), 387-395.
- Ramírez MJ, Coddington JA, Maddison WP, et al.** (2007) Linking of Digital Images to Phylogenetic Data Matrices Using a Morphological Ontology. *Syst Biol* **56**(2), 283-294.
- Sang Y-H, Hu H-C, Lu S-H, et al.** (2016) Accuracy assessment of three-dimensional surface reconstructions of in vivo teeth from cone-beam computed tomography. *Chin Med J (Engl)* **129**(12), 1464-1470.

- Santana SE.** (2018) Comparative anatomy of bat jaw musculature via diffusible iodine-based contrast-enhanced computed tomography. *Anat Rec* **301**: 267-278.
- Seymour KL.** (1999) Taxonomy, morphology, paleontology and phylogeny of the South American small cats (Mammalia: Felidae). University of Toronto Ph.D. Thesis.
- Shaheen E, Khalil W, Ezeldeen M, et al.** (2017) Accuracy of segmentation of tooth structures using 3 different CBCT machines. *Oral Surg Oral Med Oral Pathol Oral Radiol* **123(1)**, 123-128.
- Sombke A, Lipke E, Michalik P, et al.** (2015) Potential and limitations of X-Ray micro-computed tomography in arthropod neuroanatomy: A methodological and comparative survey. *J Comp Neurol* **523**, 1281-1295.
- Stephenson RS, Boyett MR, Hart G, et al.** (2012) Contrast enhanced micro-computed tomography resolves the 3-dimensional morphology of the cardiac conduction system in mammalian hearts. *PLoS ONE* **7(4)**, e35299.
- Tahara R, Larsson HCE.** (2013) Quantitative analysis of microscopic X-ray computed tomography imaging: Japanese quail embryonic soft tissues with iodine staining. *J Anat* **223**, 297-310.
- Tsai HP, Holliday CM.** (2011) Ontogeny of the alligator cartilage transiliens and its significance for sauropsid jaw muscle evolution. *PLoS ONE* **6(9)**, e24935.
- Vickerton P, Jarvis J, Jeffery N.** (2013) Concentration-dependent specimen shrinkage in iodine-enhanced microCT. *J Anat* **223**, 185-193.
- Vickerton P, Jarvis J, Gallagher JA, et al.** (2014) Morphological and histological adaptation of muscle and bone to loading induced by repetitive activation of muscle. *Proc Roy Soc B* **281**, 20140786.

- Whyms BJ, Vorperian HK, Gentry LR, et al.** (2013) The effect of CT scanner parameters and 3D volume rendering techniques on the accuracy of linear, angular, and volumetric measurements of the mandible. *Oral Surg Oral Med Oral Pathol Oral Radiol* **115(5)**, 682-691.
- Wong MD, Dorr AE, Walls JR, et al.** (2012) A novel 3-D mouse embryo atlas based on micro-CT. *Development* **129**, 3248–3256.
- Wong MD, Maezawa Y, Lerch JP, et al.** (2014) Automated pipeline for anatomical phenotyping of mouse embryos using micro-CT. *Development* **141**, 2533-2541.
- Wong MD, Spring S, Henkelman RM.** (2013) Structural stabilization of tissue for embryo phenotyping using micro-CT with iodine staining. *PLoS ONE* **8**, e84321.
- Yuen AHL, Tsui HCL, Kot BCW.** (2017) Accuracy and reliability of cetacean cranial measurements using computed tomography three dimensional volume rendered images. *PLoS ONE* **12(3)**, e0174215

Table 1

Scanning Parameters

Parameter	Unstained	Stained
Date	25 March 2016	13 May 2016
Scanner	NSI	NSI
Source	Fein Focus High Power	Fein Focus High Power
Voltage	150 kV	150 kV
Amperage	0.10 mA	0.14 mA
Filter	None	None
Detector	Perkin Elmer	Perkin Elmer
Source to object	192.0 mm	205.0 mm
Source to detector	1316.774 mm	1316.772 mm
Beam-hardening correction	0.1	0.1
Voxel size	45.4 μm	25.6 μm
Total slices	938	1905

Table 2

Volume measurements by method

Archimedes Method	Specific Muscle Density Method
Parotid gland (right)	Anterior digastric (left)
Submandibular gland (right)	Posterior digastric (left)
Digastric, including digastric sling (right)	Superficial masseter (left)
Superficial masseter (right)	Deep masseter (left)
Deep masseter (right)	Zygomatico-mandibularis (left)
Zygomatico-mandibularis (right)	Superficial temporalis (left)
Temporalis (right)	Deep temporalis (left)
Sublingual gland (left)	Zygomatic temporalis (left)
Deep medial pterygoid (right)	Superficial medial pterygoid (left)
Superficial medial pterygoid (right)	Deep medial pterygoid (left)
Lateral pterygoid (right)	Lateral pterygoid (left)
Optic disk (right)	
Mandible	

Table 3

Mandible volumes and grayscale value data

	Volume (mm ³)	Minimum Grayscale Values	Maximum Grayscale Values
Gross	500	-	-
Unstained	503.00	64	255
DiceCT	408.48	54	187

Table 4

Volumes and percentages of mastication muscles for gross dissection and diceCT

Muscle	Muscle volume (density) (mm ³)*	diceCT (mm ³)*	Dissection percent muscle volume (%)*	diceCT percent muscle volume (%)*	Muscle volume (Archimedes) (mm ³)†	diceCT (mm ³) †	Dissection percent muscle volume (%)†	diceCT percent muscle volume (%)†
Digastric (total)	43.544	43.977	4.55	3.82	81.498	50.1918	5.71	3.84
Anterior Digastric	33.131	29.2988	76.09	66.62	-	-	-	-
Posterior Digastric	10.413	14.6781	23.91	33.38	-	-	-	-
Medial Pterygoid	80.462	130.5093	8.41	11.34	118.920	109.7875	8.34	8.39
Lateral Pterygoid	68.156	75.2435	7.12	6.54	124.742	70.9109	8.75	5.42
Temporalis (total)	450.587	579.163	47.08	50.31	686.911	761.0719	48.16	58.16

(continued)

Muscle	Muscle volume (density) (mm ³)*	diceCT (mm ³)*	Dissection percent muscle volume (%)*	diceCT percent muscle volume (%)*	Muscle volume (Archimedes) (mm ³)†	diceCT (mm ³) †	Dissection percent muscle volume (%)†	diceCT percent muscle volume (%)†
Deep Temporalis	251.799	328.3123	55.88	56.69	-	-	-	-
Superficial Temporalis	156.191	165.2522	34.66	28.53	-	-	-	-
Zygomatic Temporalis	42.598	85.5985	9.45	14.78	-	-	-	-
Masseter (total)	218.667	225.176	22.85	19.56	305.201	236.863	21.40	18.10
Deep Masseter	31.238	59.929	14.29	26.61	80.666	60.2708	26.43	25.45
Superficial Masseter	187.429	165.2469	85.71	73.39	224.535	176.5918	73.57	74.55
Zygomatoco-mandibularis	95.608	97.0579	9.99	8.43	108.941	79.7349	7.64	6.09

(continued)

Muscle	Muscle volume (density) (mm ³)*	diceCT (mm ³)*	Dissection percent muscle volume (%)*	diceCT percent muscle volume (%)*	Muscle volume (Archimedes) (mm ³)†	diceCT (mm ³) †	Dissection percent muscle volume (%)†	diceCT percent muscle volume (%)†
Total	957.024	1151.127	100	100	1426.213	1308.560	100	100

*Note. *Data taken from left side of specimen; †Data taken from right side of specimen. Percent muscle volumes reflect the percentage of overall masticatory muscle volume (Digastric, Lateral Pterygoid, Medial Pterygoid, Temporalis, Masseter, or Zygomatico-mandibularis), or the percentage that a part of the muscle makes up, of the whole muscle*



Figure 3. Common marmoset head used in study. The previously frozen head of a male common marmoset, *Callithrix jacchus*.

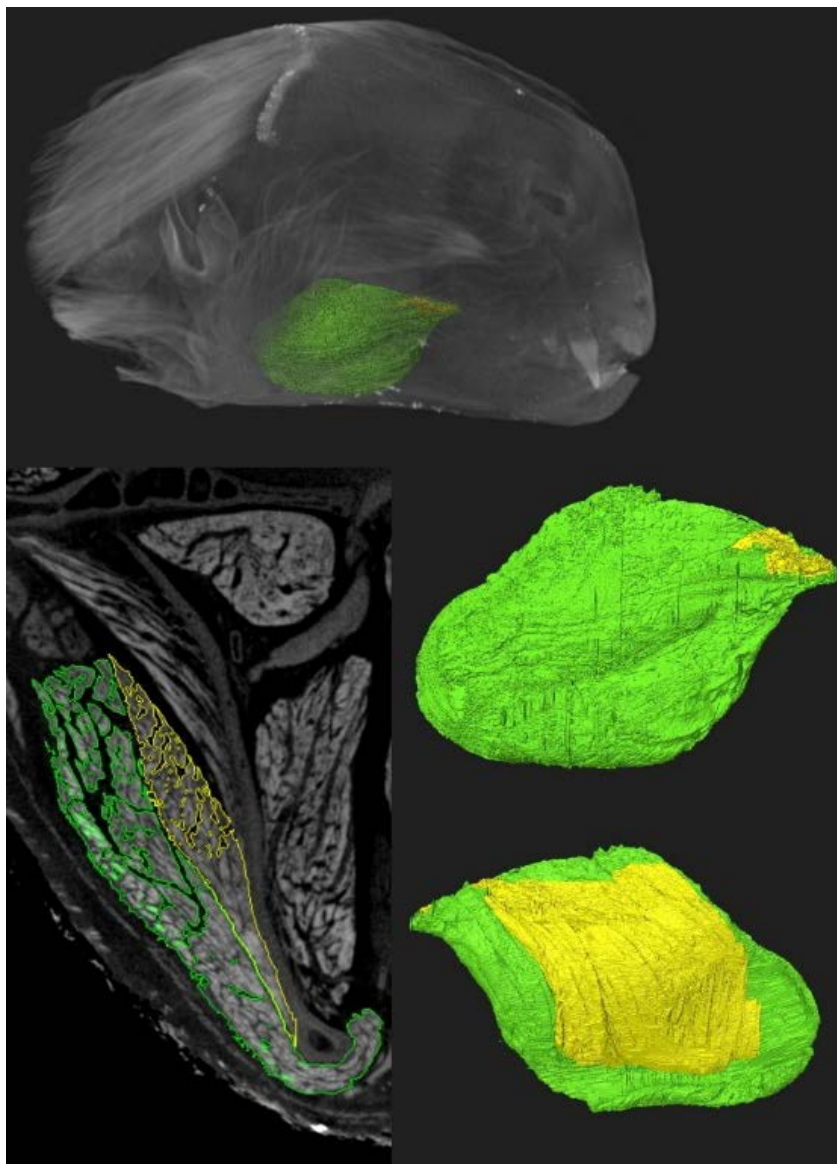


Figure 4. Example segmentation and rendering. Segmented deep masseter (yellow) and superficial masseter (green) (bottom left), then rendered together (bottom right) and location in head (top).



Figure 5. Partially dissected common marmoset. Study specimen near the beginning of the gross dissection, having only had the skin from the right side of its face removed.

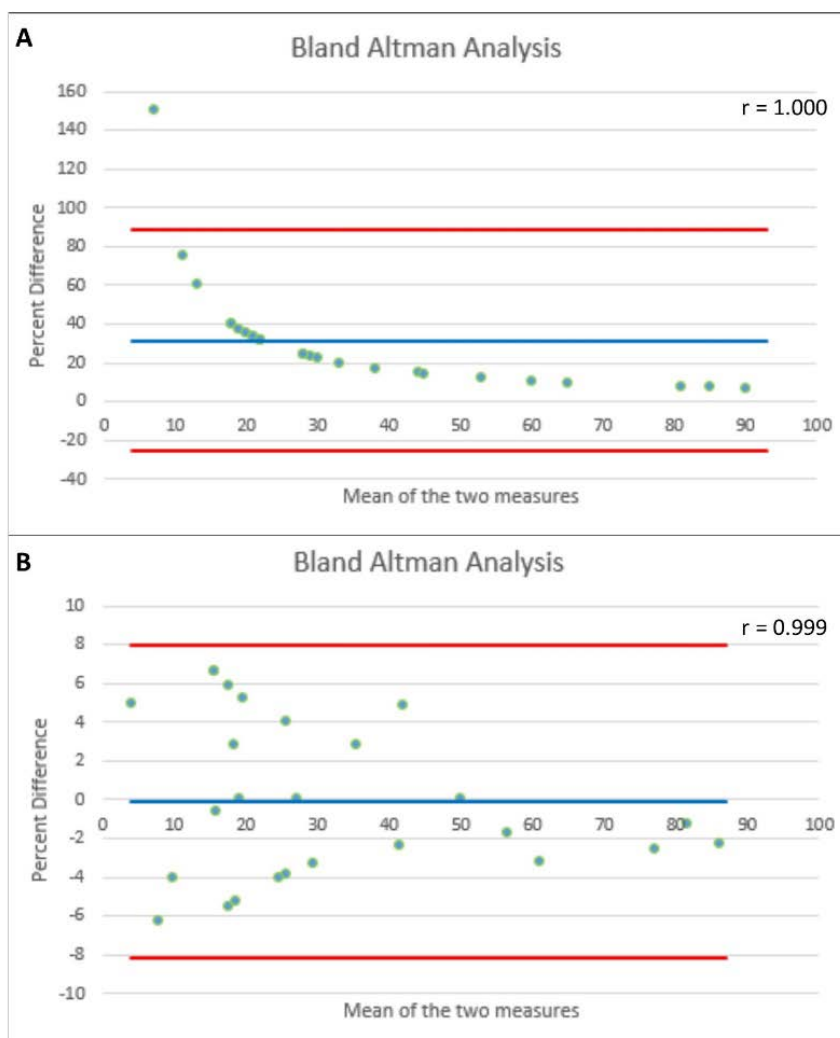


Figure 6. Example Bland-Altman analyses. The green points represent data points plotting the mean of the measures on the x-axis, and the percent difference in those measurements along the y-axis. The blue line represents the mean line of equality, calculated as the mean percent difference of all data pairs. The red lines are the 95% confidence intervals around the mean line of equality. (A) Example of a Bland-Altman analysis with perfectly correlated data that would not support the methods being comparable. (B) Example of a Bland-Altman analysis with very highly correlated data that would support the methods being comparable.

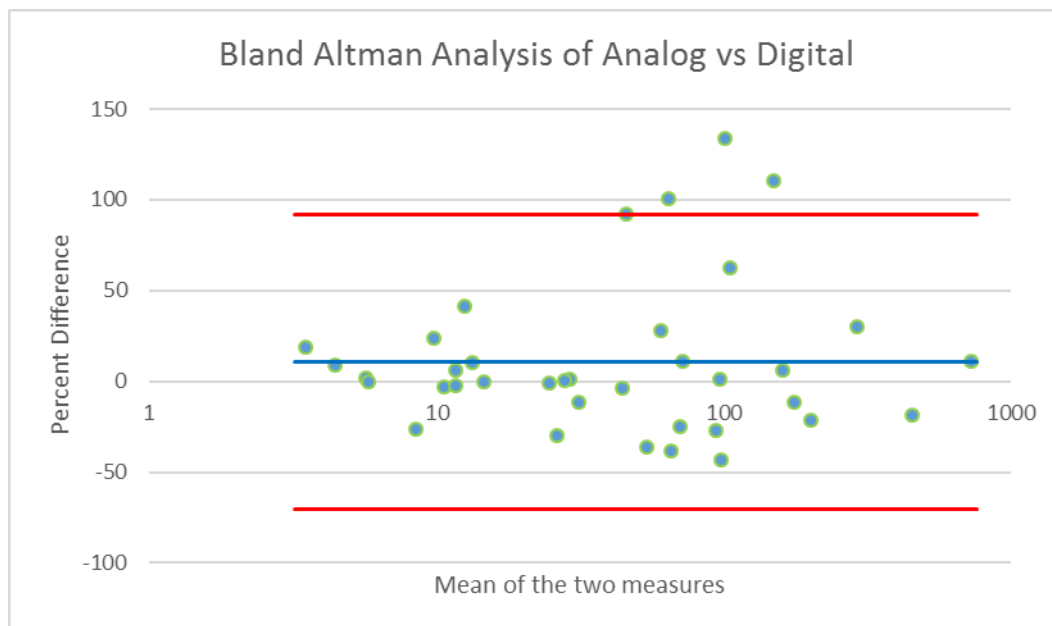


Figure 7. Bland Altman analysis of gross dissection (analog) compared to diceCT (digital) measurements. The blue line represents the mean line of equality, calculated as the mean percent difference of all data pairs. The red lines are the 95% confidence intervals around the mean line of equality. Note the logarithmic scale of the x-axis to better visualize all data.

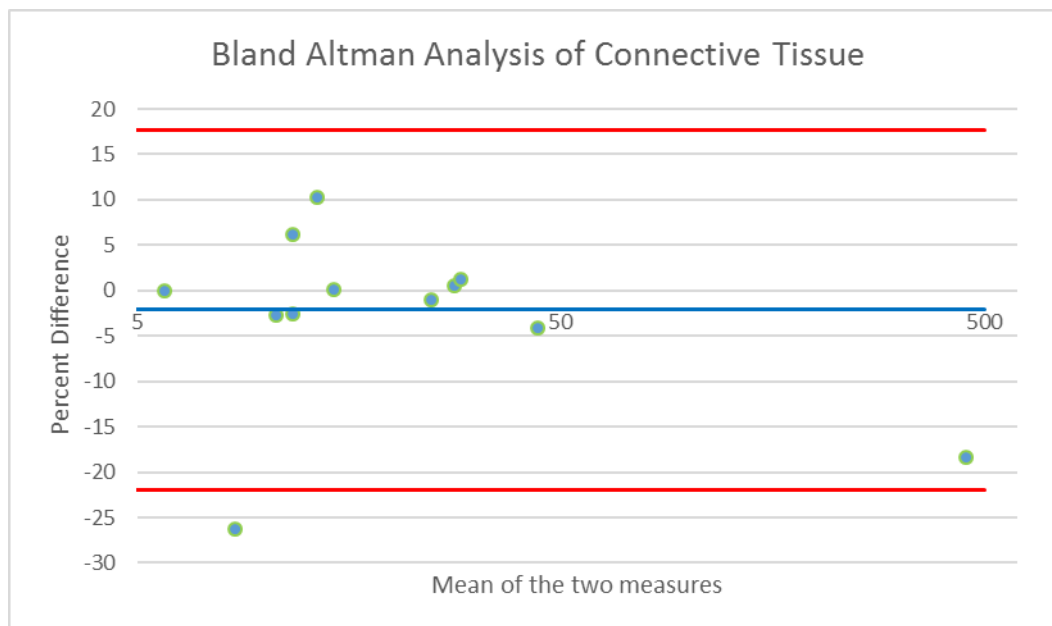


Figure 8. Bland Altman analysis of connective tissue data. The blue line represents the mean line of equality, calculated as the mean percent difference of all data pairs. The red lines are the 95% confidence intervals around the mean line of equality. Note the logarithmic scale of the x-axis to better visualize all data.

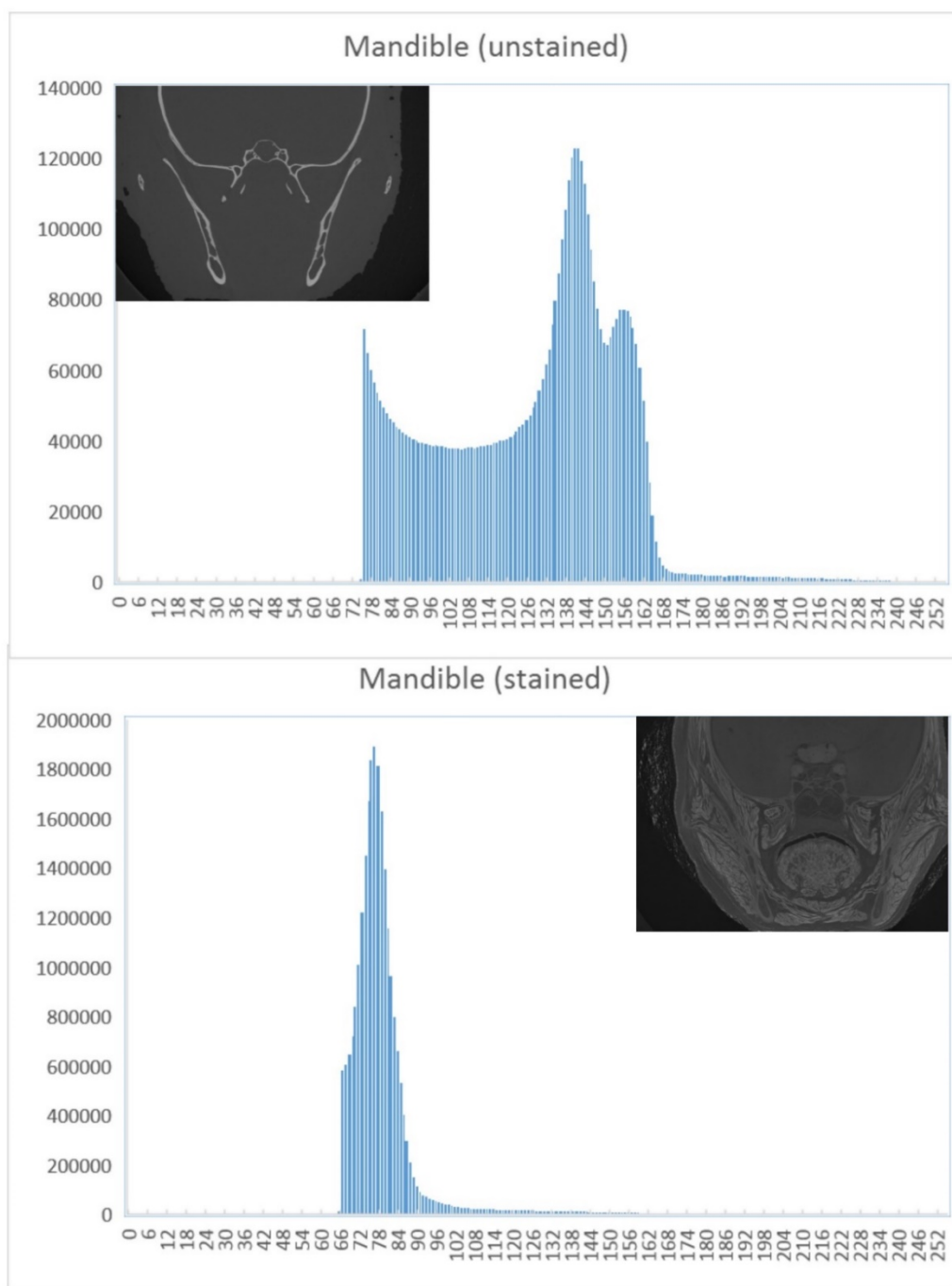


Figure 9. Histogram comparison of grayscale values between the stained and unstained mandible.

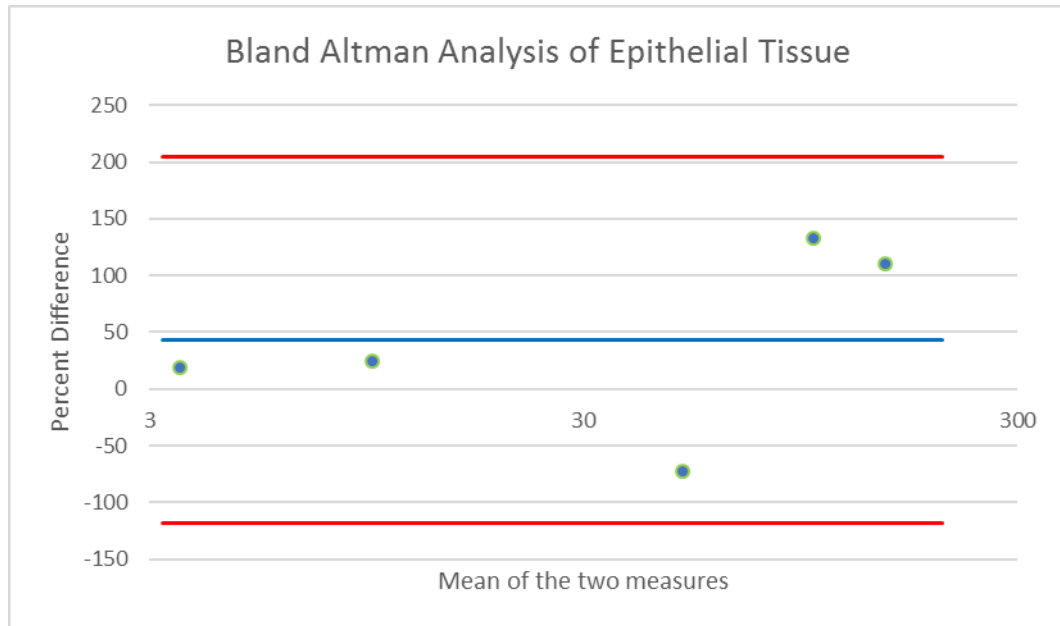


Figure 10. Bland Altman analysis of epithelial tissue measurements. The blue line represents the mean line of equality, calculated as the mean percent difference of all data pairs. The red lines are the 95% confidence intervals around the mean line of equality. Note the logarithmic scale of the x-axis to better visualize all data.

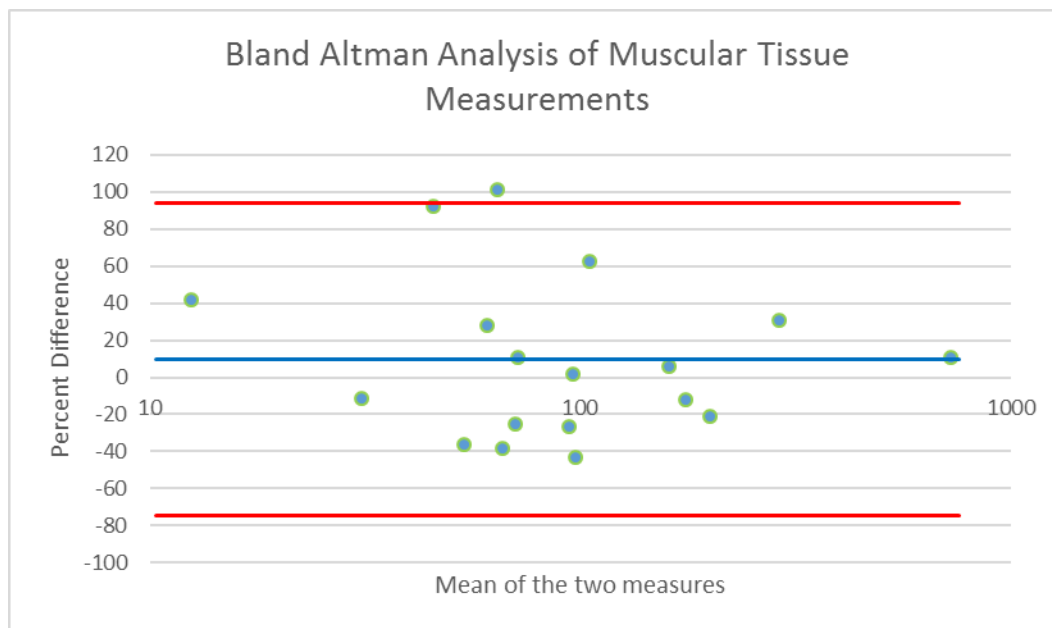


Figure 11. Bland Altman analysis of muscle tissue measurements. The blue line represents the mean line of equality, calculated as the mean percent difference of all data pairs. The red lines are the 95% confidence intervals around the mean line of equality. Note the logarithmic scale of the x-axis to better visualize all data.

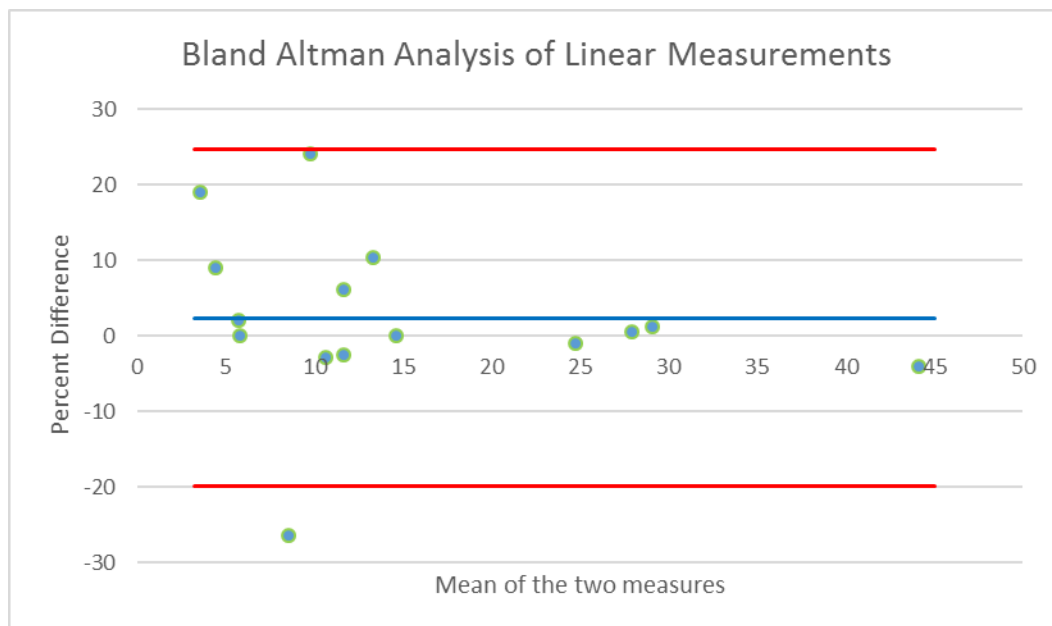


Figure 12. Bland Altman analysis of linear measurements. The blue line represents the mean line of equality, calculated as the mean percent difference of all data pairs. The red lines are the 95% confidence intervals around the mean line of equality.

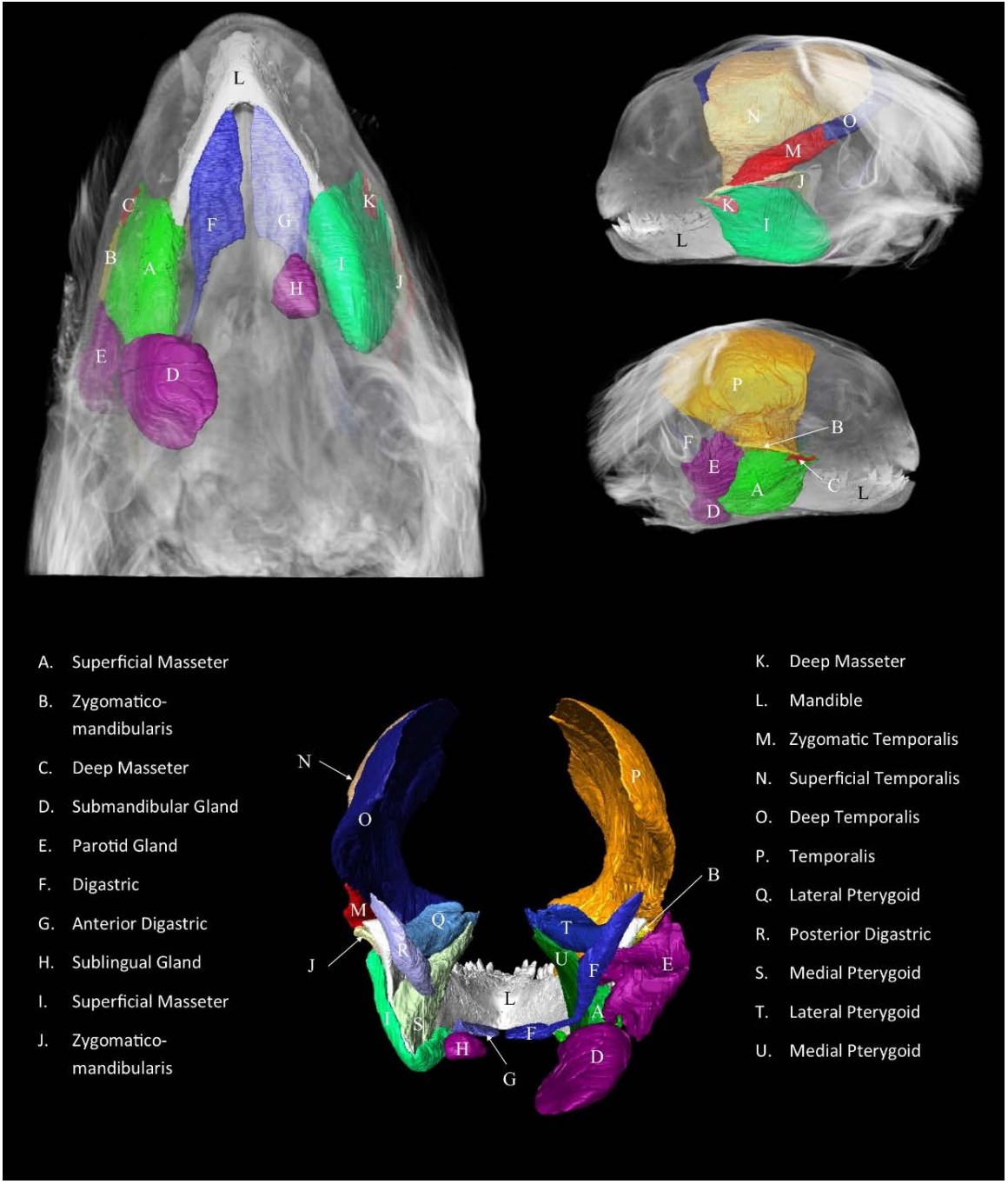


Figure 13. Muscle, gland, and mandible reconstructions. DiceCT based 3D reconstructions of the muscles, glands, and bone used to acquire volumetric data, showing *in situ* locations.

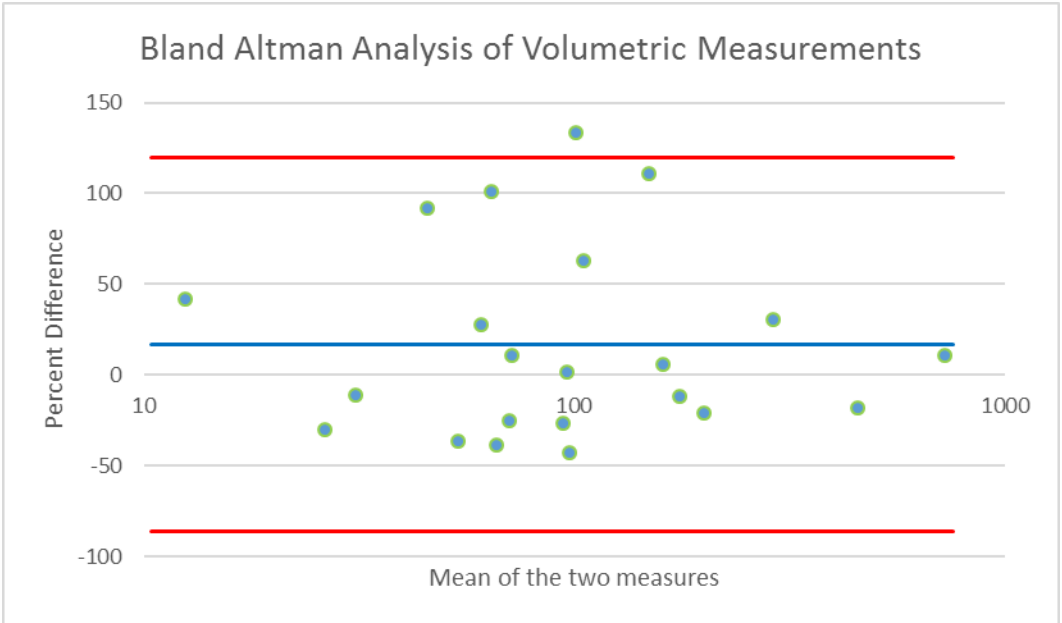


Figure 14. Bland Altman analysis of volumetric data. The blue line represents the mean line of equality, calculated as the mean percent difference of all data pairs. The red lines are the 95% confidence intervals around the mean line of equality. Note the logarithmic scale of the x-axis to better visualize all data.

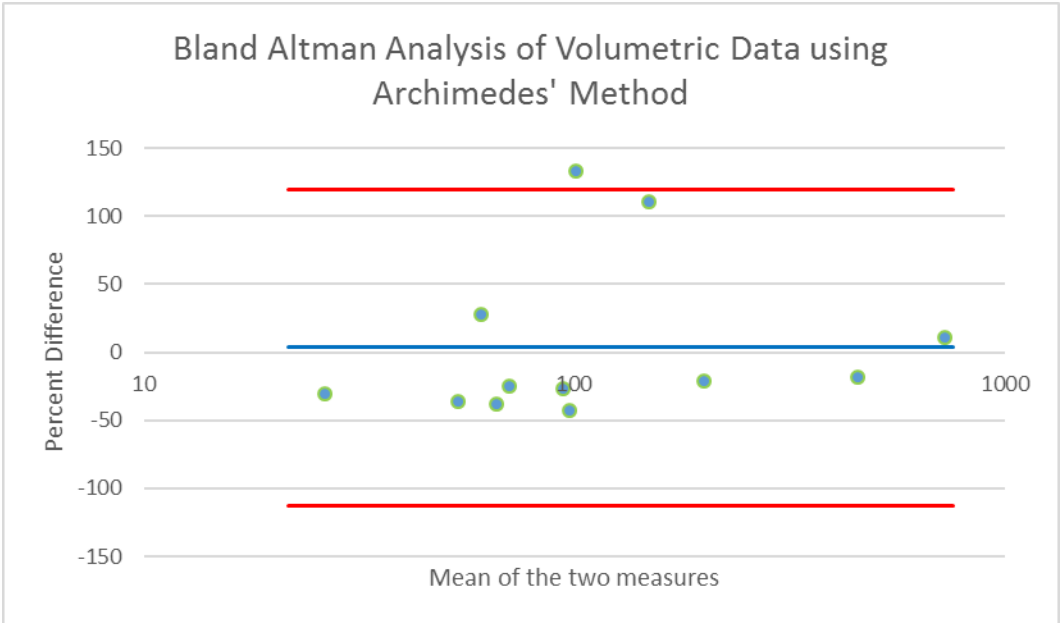


Figure 15. Bland Altman analysis of volumetric data obtained using Archimedes' method. Blue line representing the mean line of equality, calculated as the mean percent difference of all data pairs. The red lines are the 95% confidence intervals around the mean line of equality. Note the logarithmic scale of the x-axis to better visualize all data.

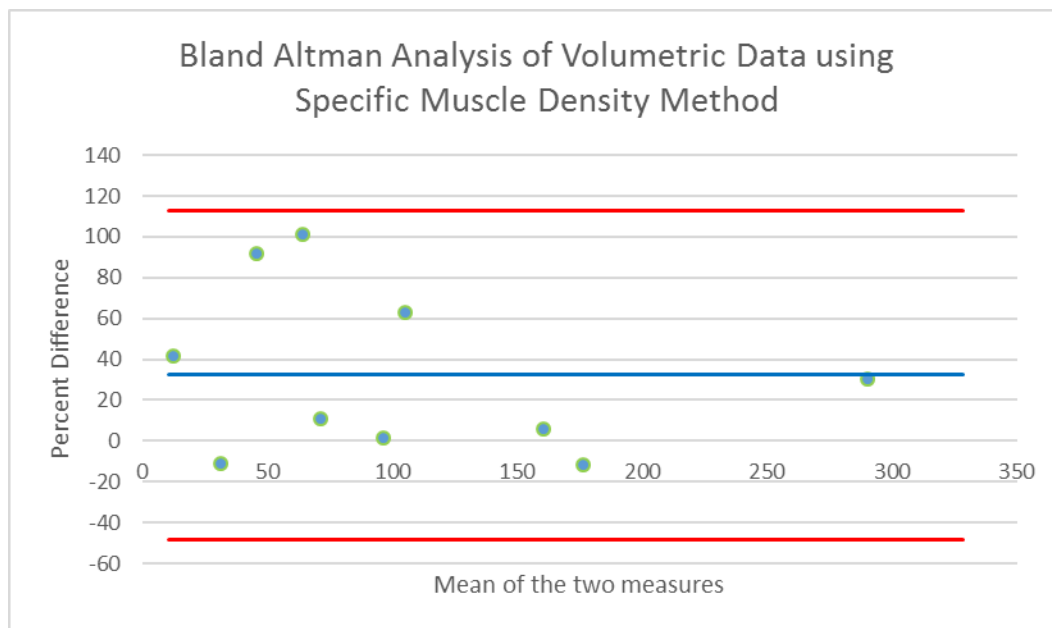


Figure 16. Bland Altman analysis of volumetric data obtained using the specific muscle density method. Blue line representing the mean line of equality, calculated as the mean percent difference of all data pairs. The red lines are the 95% confidence intervals around the mean line of equality.

CHAPTER III

A recalibration of the specific density of muscle in the era of diceCT

This thesis follows the style and format of *Journal of Anatomy*.

Abstract

The use of diffusible iodine-based contrast-enhanced computed tomography (diceCT) has revolutionized the study of in situ soft tissues in three dimensions. Differences have been reported in the measurements produced in diceCT and gross dissection. The differences reported in these two methods are hypothesized here to be due, in part, to the use of muscle density constants. To this end, the head of a common marmoset, *Callithrix jacchus*, was stained in 2.5% Lugol's solution for 37 days, with fresh solution supplied after 20 days, and studied digitally. Prior to dissection, the head was CT scanned. Amira 5.6 was used to digitally segment and isolate mastication muscles. Muscle density was recorded using masses from traditional dissection and volumes from diceCT. Based on one sample t testing and regression analyses, mammalian muscle density is more varied and less constant than previously reported and used. New constants, recalibrated for diceCT, are proposed with the caveat they only be used when dissection cannot be performed. If dissection can be performed, it is advisable to do so because muscle density is variable.

Keywords: Diffusible iodine-based contrast-enhanced computed tomography (diceCT); Gross dissection; Three-dimensional imaging; Muscle density; *Callithrix jacchus*

A recalibration of the specific density of muscle in the era of diceCT

Introduction

Diffusible iodine-based contrast-enhanced computed tomography (“diceCT”) (sensu Gignac et al. 2016) has grown rapidly as a tool for researchers since its first use by Metscher (2009a,b). With the advent of diceCT, new biomechanical models using *in situ* data are generated for investigating functional morphology and evolutionary relationships (Cox et al. 2011, 2012; Dickinson et al. 2018; Santana, 2018). These studies use physiological cross-sectional area (PCSA) in model building. Physiological cross-sectional area is calculated by dividing the mass of a muscle by the product of its fascicle length and a constant muscle density (Perry et al. 2011). The muscle densities used are typically 1.0564 g/cm^3 (Murphy & Beardsley, 1974) or 1.06 g/cm^3 (Mendez & Keys, 1960). Both are traditionally referred to as mammalian muscle densities, because the densities were derived from mammalian specimens (Mendez & Keys, 1960; Murphy & Beardsley, 1974). These values are used in calculations of PCSA in primates (Taylor & Vinyard, 2004; Eng et al. 2009; Taylor et al. 2009; Perry et al. 2011, 2014; Hartstone-Rose et al. 2018), felids (Hartstone-Rose et al. 2012), canids (Dickinson et al. 2018) bats (Herrel et al. 2008; Santana et al. 2010; Santana, 2018), and rodents (Rupert et al. 2015). These muscle densities are used to transform muscle masses into volumes for comparison with diceCT produced volumes (Baverstock et al. 2013). The reverse is also true, and these muscle densities are used to convert diceCT volumes to muscle mass for comparison with published data (Cox & Jeffery, 2011; Cox & Faulkes, 2014). While generally used for mammals, Bribiesca-Contreras & Sellers (2017) used the density of 1.06 g/cm^3 (Mendez & Keys, 1960) to convert the masses of bird muscles to volumes for

comparison to diceCT volumes. DiceCT can also visualize fascicles, and thus their lengths (Jeffery et al. 2011), meaning that all components of PCSA can be calculated using diceCT. However, diceCT provides a significantly higher PCSA estimate than traditional dissection (Santana, 2018). Muscle volumes computed between diceCT and traditional gross dissection have also been found to be significantly different (See Chapter II). I hypothesize this difference between diceCT and gross dissection to be due to the use of constant muscle density in calculations that is not calibrated for diceCT.

Methods

Staining. A frozen male common marmoset (*Callithrix jacchus*) that died in a zoo was chosen for its size which is optimal for both scanning and dissection. A head was selected to investigate the masticatory muscles that are commonly used to compute PCSA. The head was fixed in 10% formalin, then submerged in 2.5% I₂KI (Lugol's solution) for a total of 37 days. Lugol's solution was chosen over iodine in ethanol, due to the improved visualization of muscle fibers (Li et al. 2016). High concentrations of Lugol's solution can cause dramatic shrinkage in muscle tissue (Vickerton et al. 2013), so a low concentration was chosen to help minimize this effect. Lugol's solution was replaced after 20 days, a multiple stage staining method used to improve contrast (Jeffrey et al. 2011; Li et al. 2015; Kupczik et al. 2015; Gignac et al. 2016). Experts at the scanning facility kept the specimen in Lugol's solution until it was believed the highest quality images for analysis could be obtained. No Institutional Animal Care and Use Committee approval was necessary for this experiment, because the common marmoset was deceased. The specimen was chosen for its size that allows for both scanning and dissection.

Scanning. Scanning was performed at The University of Texas High-Resolution X-ray Computed Tomography Facility (UTCT) on a North Star Imaging (NSI) scanner, using the ultra-high-resolution subsystem. An initial scan, prior to iodine staining, at 150kV, 0.1 mA, and voxel size 45.4 μm (following Gignac et al. 2016) was performed as bone shows up best prior to staining procedures (Baverstock et al. 2013; Gignac et al. 2016; Li et al. 2016). During staining, test scans were performed every two days to ensure that the specimen was not oversaturated (Gignac et al. 2016). A final scan, once appropriately saturated, was performed at 150kV, 0.14mA, and voxel size 25.6 μm (following Gignac et al. 2016; Table 1). Difference in voxel size is seen to be insignificant to volumetric reconstructions when voxel size is kept at or below 76 μm (Damstra et al. 2010; Maret et al. 2012, 2014; Sang et al. 2016). Both scans produced 16-bit TIFF and 8-bit JPEG image files of the slices.

Segmentation. The 8-bit dataset was selected for use based on computational power and the advice from the UTCT operators. Using the 8-bit JPEG image files, muscles were digitally segmented and rendered to be measured. Segmentation is the selection of pixels from each slice of the scan to be reconstructed into a three-dimensional model (Figure 4). Using the paintbrush and magic wand tools, segmentation was completed in the segmentation editor of Amira 5.6. The paintbrush tool allowed for manual selection of voxels to be assigned to defined as a specific muscle. The magic wand used differences in greyscale values to approximate borders between structures.

Automatic thresholding and segmenting procedures were not used as they are known to cause both false-positive and false-negative voxels (Wong et al. 2012; Balanoff et al. 2015). A false-positive voxel would be one that has been segmented as a one

muscle when it is not part of that muscle, while a false-negative voxel would be one that should be segmented as a particular muscle but has not been segmented as that muscle, if at all.

Rendering. Volume Rendering, for viewing segmented structures and obtaining images was done in Amira 5.6 using the surface generator, volren and isosurface tools without any smoothing effects outside of the default programming, (Figure 4).

Measurements were taken using the material statistics function for volumes (Appendix). Images of rendered muscles were exported using the snapshot tool, in order to create figures.

Gross Dissection. Dissection of structures of interest was performed at the University of South Carolina by Carissa Leischner, a researcher with experience dissecting primates, to ensure accurate identifications and procedures (Hartstone-Rose et al. 2018; Leischner et al. 2018). Following removal of the skin, the most external muscles were removed (e.g. superficial masseter, deep masseter, etc.) followed by progressively more internal structures (e.g. temporalis, medial pterygoid, lateral pterygoid, etc.) until all muscles of interest were removed. This took place on the left side of the head. Removed muscles were massed using a digital scale (Table 5).

Previously Published Data. Data from studies that collected masses in gross dissection and volumes in diceCT (Baverstock et al. 2013; Bribiesca-Contreras & Sellers, 2017) were included to increase sample size and variety. Values in both papers had to be back-calculated from published volumes to masses using the cited density constant (Table 5). Baverstock et al. (2013) used 1.0546 g/cm³ (Murphy & Beardsley, 1974), while Bribiesca-Contreras & Sellers (2017) used 1.06 g/cm³ (Mendez & Keys, 1960).

Statistics. Using the muscle mass from gross dissection and the volume from diceCT, a muscle density for each muscle was computed (Table 5). Mean muscle density was calculated for the overall dataset, each individual study, and for mammalian muscles only (Table 6). Additionally, two large outliers were removed, and means for the affected groups were recomputed, because the two data points were greater than two standard deviations (SD) away from the mean. A two-tailed one-sample t test was used to test how each set of muscle densities compared to the previously established 1.0546 g/cm^3 (Murphy & Beardsley, 1974), and 1.06 g/cm^3 (Mendez & Keys, 1960). For the one-sample t test, each of the previously established values acts as a hypothetical mean, and the test evaluates how likely it is that that mean would fit inside of the new dataset. This t test was chosen since there was only one mean value to compare to the muscle density data collected. A regression analysis was also performed, comparing the muscle mass to diceCT volume, the slope of which, will yield the newly calibrated muscle density constant.

Results

Using the muscles traditionally and digitally dissected from the *Callithrix jacchus*, along with previously published data (Baverstock et al. 2013; Bribiesca-Contreras & Sellers, 2017), muscle density was calculated ($n=44$). One sample t tests show a significant difference between the muscle density calculated from the *Callithrix jacchus* for this study (Table 6) and both of the previously established muscle densities of 1.0546 g/cm^3 (Murphy & Beardsley, 1974), and 1.06 g/cm^3 (Mendez & Keys, 1960). There was also a significant difference when looking at all available mammalian muscle

data (Baverstock et al. 2013; This study) when compared to previously established values (Table 6).

Data collected from avian specimens from Bribiesca-Contreras & Sellers (2017), as well as the overall dataset (data collected from both previously mentioned studies and this one) were not found to be statistically similar (Table 6). However, there were two muscles that had reported densities of over 2.3 g/cm^3 (Table 5), more than twice as dense as previously reported muscle densities (Mendez & Keys, 1960; Murphy & Beardsley, 1974). These two values were more than two standard deviations from the mean, drastically impacting the t test results (Table 6). After removing the two outliers that were more than two standard deviations from the mean, one sample t tests were recomputed for the affected datasets (All data and Bribiesca-Contreras & Sellers, 2017; Table 6). While the avian data from Bribiesca-Contreras & Sellers (2017) was still not significantly different from the previously established muscle density values, it saw a dramatic decrease in the probability that the two datasets were the same (Table 6). The whole dataset without outliers was found to be significantly different ($p=0.0118$) from the previously established muscle density of 1.0546 g/cm^3 (Murphy & Beardsley, 1974), and highly significantly different ($p=0.0096$) from the 1.06 g/cm^3 muscle density (Mendez & Keys, 1960).

Linear regressions of the muscle masses and volumes yielded slopes of 1.0555 and 0.8644 for the whole dataset and just mammalian muscles, respectively, representing the muscle densities based on regression analysis. Muscle volume and muscle mass were found to be highly correlated for both the whole dataset ($R^2=0.9614$) and for mammalian muscles ($R^2=0.9136$; *Figure 17*). Over 90% of the variation in muscle mass can be

explained by the variation of muscle volume in both sets of data. For muscle density to be truly constant, in all animals, or just in mammals, an R^2 value of 1 would have been expected. Avian data (Bribiesca-Contreras & Sellers, 2017) produced similar results ($m=1.0551$; $R^2=0.9624$) to the whole dataset.

Discussion

A constant muscle density is necessary to traditional gross dissection for the calculation of PCSA and muscle volumes from muscle masses. The differences in traditional gross dissection and diceCT play an unclear role in the reported differences of the two methods, though the constant muscle density may be one reason. Identifying a mammalian muscle constant that is calibrated for use with diceCT may enable researchers to interweave diceCT and gross dissection techniques with more confidence and clarity.

In this study, muscle density was measured using masses from gross dissection and volumes computed from diceCT, which was found to be significantly different from previously published values, supporting other work that has found significant differences between diceCT and traditional gross dissection (Santana, 2018; See Chapter II). This was especially true for the mammalian muscle samples, which were significantly lower than previous publications (Mendez & Keys, 1960; Murphy & Beardsley, 1974). It is important to note that Murphy & Beardsley's study was not focused on finding the density of mammalian muscle. Murphy & Beardsley were researching mechanical properties of soleus muscles in cats, and needed a density for PCSA calculations (Murphy & Beardsley, 1974). The value of 1.0564 g/cm^3 that is often cited from Murphy & Beardsley (1974) was based off a small sample size ($n=6$) of a single muscle in a single

species, meaning their data should probably not be applied to all muscles, or even to all mammalian muscles. They never suggested that it should be applied to all mammals, but it has been used in that manner since (e.g. Taylor & Vinyard, 2004; Baverstock et al. 2013). While the mammalian muscle tests presented here admittedly only come from two species, they do come from a wider collection of muscles and a larger sample size. Based on the regression analysis, a value of 0.8685 g/cm^3 should be used for mammalian muscle density, and 1.0551 g/cm^3 for avian muscle density when converting from diceCT. To confirm this Bland-Altman analyses (Altman & Bland, 1983) were performed both using both the previously established values and the newly suggested values. These tests show that the mean percent difference was reduced following the use of recalibrated muscle constants for the whole dataset, avian muscles, and especially mammalian muscles (Table 7). This decrease shows that recalibration of the muscle density constant for diceCT helps to bridge some of the current gap between gross dissection and diceCT measurements.

While this study does present a muscle density constant, it is advised that it only be used when absolutely necessary. For example, when working on a museum specimen that cannot undergo destructive testing, or if working with incredibly small muscles that cannot be dissected with precision. That constant muscle density effectively transforms the mass in the equation into a volume, allowing the formula to be simplified to muscle volume divided by fascicle length (Cox et al. 2011, 2012; Dickinson et al. 2018). DiceCT allows researchers to obtain that volume and fascicle length without dissection, though those numbers will be significantly different than the traditional means (Santana, 2018; See Chapter II). The idea of a constant muscle density is misleading. As presented here (Table 5), muscle density varies greatly, from as small as 0.2995 g/cm^3 to almost ten

times as dense as 2.7200 g/cm^3 . This wide range makes sense given that muscle pennation allows more muscle fiber to be packed into the same area, leading to higher density muscles, as well as lower density ones (Gans, 1982; Otten, 1988). It is instead suggested that, like Murphy & Beardsley (1974), Baverstock et al. (2013), Bribiesca-Contreras & Sellers (2017) and this study, researchers ideally still perform dissections to obtain muscle masses when needed, because those values are not reliant on a muscle density constant. This idea echoes those of other recent researchers using diceCT (Gignac et al. 2016; Bribiesca-Contreras & Sellers, 2017; Santana, 2018).

Iodine staining has been reported to cause shrinkage in muscles (Vickerton et al. 2013). It has also been surmised to possibly increase measured muscle mass due to the intake of the relatively heavy iodine (Santana, 2018). Neither seemed to have much of an effect on this study. For shrinkage to have played a significant role, smaller volumes would have been obtained from diceCT, leading to a larger muscle density since the denominator in the equation would be getting smaller. Since the muscle densities obtained were smaller than previous estimates, this seems to have not occurred to a significant degree. The presence of bound iodine to the muscle tissue would also have led to larger densities due to the larger mass in the numerator of the equation. Again, this seems to have not been a concern in this study given the significantly lower muscle densities (Table 6).

This study suffers from a lack of species richness and clade richness, consisting of just three species, across two classes. Sample size for mammalian data is less than ideal, but still an improvement on some previous studies. Ideally, as more specimens are analyzed using both diceCT, and gross dissection, this dataset can expand and better

address the concerns of sample size, species richness, and clade richness. Future research that expands this work could be of interest in evolutionary research, to see if there is a significant difference in muscle density among mammals. The change in muscle densities between diceCT and gross dissections could be an issue in other clades as well, just as it seems to be in mammals, warranting further investigation. The difference in muscle density based on the specific muscle needs to be investigated as well, as differences between the muscles of the same species are seen. For example, in both *Mus musculus* and *Callithrix jacchus*, superficial masseters were denser than the deep masseter. This is supported by previous diceCT work showing differential iodine staining across one muscle, meaning the muscle is not uniform throughout (Gignac & Kley, 2014). Future studies need to better delineate the differences in muscle density in gross dissection, diceCT and between the two, as muscle density seems to be misused as a constant.

Conclusions

Traditional mammalian muscle density constants of 1.0546 g/cm^3 and 1.06 g/cm^3 should not be used in conjunction with diceCT. Instead, for use with diceCT, 0.8685 g/cm^3 should be used if a conversion is absolutely necessary, as with museum samples. Otherwise, it is advised that diceCT researchers use the volumes obtained from diceCT to build and evaluate biomechanical models, such as PCSA in bite force analyses.

Acknowledgements

I thank PJ Lewis, A Hartstone-Rose, JD Daza, and JK Williams for their feedback and assistance on this manuscript. Additionally, I thank CL Leischner, JA Costa, L Rudie, C Fakhri, S Mesa, and C Basham for data acquisition assistance, The University

of Texas CT Lab for scanning support, and KM Jenkins for edits and discussions. This work was supported, in part, by the National Science Foundation (NSF IOS-15-57125).

References

- Altman DG, Bland JM.** (1983) Measurement in medicine: The analysis of method comparison studies. *J R Stat Soc* **32**, 307-317.
- Baverstock H, Jeffery NS, Cobb SN** (2013) The morphology of the mouse masticatory musculature. *J Anat* **223**, 46–60.
- Bribiesca-Contreras F, Sellers WI.** (2017) Three-dimensional visualization of the internal anatomy of the sparrowhawk (*Accipiter nisus*) forelimb using contrast-enhanced micro-computed tomography. *PeerJ* **5**: e3039.
- Cox PG, Fagan MJ, Rayfield EJ, et al.** (2011) Finite element modeling of squirrel, guinea pig and rat skulls: using geometric morphometrics to assess sensitivity. *J Anat* **219**, 696–709.
- Cox PG, Faulkes CG.** (2014) Digital dissection of the masticatory muscles of the naked mole-rat, *Heterocephalus glaber* (Mammalia, Rodentia). *PeerJ* **2**, e448.
- Cox PG, Jeffery N.** (2011) Reviewing the morphology of the jaw-closing musculature in squirrels, rats, and guinea pigs with contrast-enhanced micro-CT. *Anat Rec* **294**, 915–928.
- Cox PG, Rayfield EJ, Fagan MJ, et al.** (2012) Functional evolution of the feeding system in rodents. *PLoS ONE* **7**, e36299.
- Damstra J, Fourie Z, Huddleston Slater JJR, et al.** (2010) Accuracy of linear measurements from cone-beam computed tomography-derived surface models of different voxel sizes. *Am J Orthod Dentofacial Orthop* **137**, 16.e1-16.e6.
- Dickinson E, Stark H, Kupczik K.** (2018) Non-destructive determination of muscle architectural variables through the use of diceCT. *Anat Rec* **301**, 363-377.

- Eng CM, Ward SR, Vinyard CJ, Taylor AB.** (2009) The morphology of the masticatory apparatus facilitates muscle force production at wide jaw gaps in tree-gouging common marmosets (*Callithrix jacchus*). *J Exp Biol* **212**, 4040-4055.
- Gans C.** (1982) Fiber architecture and muscle function. *Exerc Sport Sci Rev* **10**, 160-207
- Gignac PM, Kley NJ.** (2014) Iodine-enhanced micro-CT imaging: Methodological refinements for the study of soft-tissue anatomy of post-embryonic vertebrates. *J Exp Zool B Mol Dev Evol* **322B**, 166-176.
- Gignac PM, Kley NK, Clarke JA, et al.** (2016) Diffusible iodine-based contrast-enhanced computed tomography (diceCT): an emerging tool for rapid, high-resolution, 3-D imaging of metazoan soft tissues. *J Anat* **228**, 889–909.
- Hartstone-Rose A, Deutsch AR, Leischner CL, et al.** (2018) Dietary correlates of primate masticatory muscle fiber architecture. *Anat Rec* **301(2)**, 311-324.
- Hartstone-Rose A, Perry JMG, Morrow CJ.** (2012) Bite force estimation and the fiber architecture of felid masticatory muscles. *Anat Rec* **295**, 1336-1351.
- Herrel A, De Smet A, Aguire LF, Aerts P.** (2008) Morphological and mechanical determinants of bite force in bats: do muscles matter? *J Exp Biol* **211**, 86-91
- Jeffrey NS, Stephenson RS, Gallagher JA, et al.** (2011) Micro-computed tomography with iodine staining resolves the arrangement of muscle fibres. *J Biomech* **44**, 189-192.
- Kupczik K, Stark H, Mundry R, et al.** (2015) Reconstruction of muscle fascicle architecture from iodine-enhanced microCT images: A combined texture mapping and streamline approach. *J Theor Biol* **382**, 34-43.

- Leischner CL, Crouch M, Allen KL, et al.** (2018) Scaling of primate forearm muscle architecture as it relates to locomotion and posture. *Anat Rec* **301(3)**, 484-495.
- Li Z, Clarke JA, Ketcham RA, et al.** (2015) An investigation of the efficacy and mechanism of contrast-enhanced x-ray computed tomography utilizing iodine for large specimens through experimental and simulation approaches. *BMC Physiol* **15**, 5, 16pp.
- Li Z, Ketcham RA, Yan F, et al.** (2016) Comparison and evaluation of the effectiveness of two approaches of diffusible iodine-based contrast- enhanced computed tomography (diceCT) for avian cephalic material. *J Exp Zool B Mol Dev Evol* **00B**, 1–11.
- Maret D, Peters OA, Galibourg A, et al.** (2014) Comparison of the accuracy of 3-dimensional cone-beam computed tomography and micro-computed tomography reconstructions by using different voxel sizes. *J Endod* **39**, 394-397.
- Maret D, Telmon N, Peters OA, et al.** (2012) Effect of voxel size on the accuracy of 3D reconstructions with cone beam CT. *Dentomaxillofac Radiol* **41**, 649-655.
- Mendez J, Keys A.** (1960) Density and composition of mammalian muscle. *Metabolism* **9**, 184-188.
- Metscher BD.** (2009a) Micro-CT for developmental biology: a versatile tool for high-contrast 3-D imaging at histological resolutions. *Dev Dyn* **238**, 632–640.
- Metscher BD.** (2009b) Micro-CT for comparative morphology: simple staining methods allow high-contrast 3D imaging of diverse non-mineralized animal tissues. *BMC Physiol* **9**, 11.

- Murphy RA, Beardsley AC.** (1974) Mechanical properties of the cat soleus muscle in situ. *Am J Physiol* **227(5)**, 1008-1013
- Otten E.** (1988) Concepts and models of functional architecture in skeletal muscle. *Exerc Sport Sci Rev* **16**, 98-138.
- Perry JMG, Hartstone-Rose A, Wall CE.** (2011) The jaw adductors of strepsirrhines in relation to body size, diet, and ingested food size. *Anat Rec* **294**, 712-728.
- Perry JMG, Macneill KE, Heckler AL, et al.** (2014) Anatomy and adaptations of the chewing muscles in *Daubentonia* (Lemuriformes). *Anat Rec* **297**, 308-316.
- Rupert JE, Rose JA, Organ JM, Butcher MT.** (2015) Forelimb muscle architecture and myosin isoform composition in the groundhog (*Marmota monax*). *J Exp Biol* **218**, 194-205.
- Sang Y-H, Hu H-C, Lu S-H, et al.** (2016) Accuracy assessment of three-dimensional surface reconstructions of in vivo teeth from cone-beam computed tomography. *Chin Med J (Engl)* **129(12)**, 1464-1470.
- Santana SE.** (2018) Comparative anatomy of bat jaw musculature via diffusible iodine-based contrast-enhanced computed tomography. *Anat Rec* **301**: 267-278.
- Santana SE, Dumont ER, Davis JL.** (2010) Mechanics of bite force production and its relationship to diet in bats. *Funct Ecol* **24**, 776-784.
- Taylor AB, Eng CM, Anapol F, Vinyard C.** (2009) The functional correlates of jaw-muscle fiber architecture in tree-gouging and nongouging callitrichid monkeys. *Am J Phys Anthropol* **139**, 353-367.

Taylor A, Vinyard C. (2004) Comparative analysis of masseter fiber architecture in tree-gouging (*Callithrix jacchus*) and nongouging (*Saguinus oedipus*) callitrichids. *J Morphol*

Vickerton P, Jarvis J, Jeffery N. (2013) Concentration-dependent specimen shrinkage in iodine-enhanced microCT. *J Anat* **223**, 185-193.

Table 5

Muscles analyzed, including masses, volumes, and densities

Muscle	Species	Study	Mass (g)	diceCT Volume (mm ³)	Muscle Density (g/cm ³)
Anterior Digastric	<i>Callithrix jacchus</i>	This study	0.035	29.30	1.1945
Posterior Digastric	<i>Callithrix jacchus</i>	This study	0.011	14.68	0.7493
Superficial Masseter	<i>Callithrix jacchus</i>	This study	0.198	165.25	1.1982
Deep Masseter	<i>Callithrix jacchus</i>	This study	0.033	59.93	0.5506
Zygomatico- mandibularis	<i>Callithrix jacchus</i>	This study	0.101	97.06	1.0406
Superficial Temporalis	<i>Callithrix jacchus</i>	This study	0.165	165.25	0.9985
Deep Temporalis	<i>Callithrix jacchus</i>	This study	0.266	328.31	0.8102

(continued)

Muscle	Species	Study	Mass (g)	diceCT Volume (mm ³)	Muscle Density (g/cm ³)
Zygomatic Temporalis	<i>Callithrix jacchus</i>	This study	0.045	85.60	0.5257
Medial Pterygoid	<i>Callithrix jacchus</i>	This study	0.085	130.51	0.6513
Lateral Pterygoid	<i>Callithrix jacchus</i>	This study	0.072	75.24	0.9569
Superficial masseter	<i>Mus musculus</i>	Baverstock et al. 2013	0.068	58.5	1.1557
Deep masseter	<i>Mus musculus</i>	Baverstock et al. 2013	0.106	101.89	1.0368
Zygomatico mandibularis	<i>Mus musculus</i>	Baverstock et al. 2013	0.026	26.92	0.9811
Temporalis	<i>Mus musculus</i>	Baverstock et al. 2013	0.063	68.63	0.9236

(continued)

Muscle	Species	Study	Mass (g)	diceCT Volume (mm ³)	Muscle Density (g/cm ³)
External pterygoid	<i>Mus musculus</i>	Baverstock et al. 2013	0.011	14.49	0.7291
Internal pterygoid	<i>Mus musculus</i>	Baverstock et al. 2013	0.034	35.38	0.9555
<i>abductor alulae</i>	<i>Accipiter nisus</i>	Bribiesca-Contreras & Sellers, 2017	0.011	19	0.5958
<i>abductor digiti majoris</i> (ABDM closest)	<i>Accipiter nisus</i>	Bribiesca-Contreras & Sellers, 2017	0.040	23	1.7227
<i>adductor alulae</i>	<i>Accipiter nisus</i>	Bribiesca-Contreras & Sellers, 2017	0.013	21	0.6289

(continued)

Muscle	Species	Study	Mass (g)	diceCT Volume (mm ³)	Muscle Density (g/cm ³)
<i>biceps brachii</i>	<i>Accipiter nissus</i>	Bribiesca- Contreras & Sellers, 2017	0.900	754	1.1936
<i>brachialis</i>	<i>Accipiter nissus</i>	Bribiesca- Contreras & Sellers, 2017	0.032	47	0.6825
<i>deltoides major</i>	<i>Accipiter nissus</i>	Bribiesca- Contreras & Sellers, 2017	1.009	947	1.0659
<i>ectepicondylo ulnaris</i>	<i>Accipiter nissus</i>	Bribiesca- Contreras & Sellers, 2017	0.114	139	0.8212
<i>extensor brevis alulae</i>	<i>Accipiter nissus</i>	Bribiesca- Contreras & Sellers, 2017	0.007	6	1.1006

(continued)

Muscle	Species	Study	Mass (g)	diceCT Volume (mm ³)	Muscle Density (g/cm ³)
<i>extensor carpi ulnaris</i>	<i>Accipiter nissus</i>	Bribiesca- Contreras & Sellers, 2017	0.373	137	2.7200
<i>extensor digitorum communis</i>	<i>Accipiter nissus</i>	Bribiesca- Contreras & Sellers, 2017	0.162	154	1.0537
<i>extensor longus alulae</i>	<i>Accipiter nissus</i>	Bribiesca- Contreras & Sellers, 2017	0.092	96	0.9532
<i>extensor longus digiti majoris</i>	<i>Accipiter nissus</i>	Bribiesca- Contreras & Sellers, 2017	0.072	39	1.8384
<i>flexor alulae</i>	<i>Accipiter nissus</i>	Bribiesca- Contreras & Sellers, 2017	0.008	18	0.4717

(continued)

Muscle	Species	Study	Mass (g)	diceCT Volume (mm ³)	Muscle Density (g/cm ³)
<i>flexor carpi ulnaris</i>	<i>Accipiter nissus</i>	Bribiesca- Contreras & Sellers, 2017	0.567	578	0.9809
<i>flexor digiti minoris (FDML)</i>	<i>Accipiter nissus</i>	Bribiesca- Contreras & Sellers, 2017	0.051	22	2.3156
<i>flexor digitorum profundus</i>	<i>Accipiter nissus</i>	Bribiesca- Contreras & Sellers, 2017	0.082	107	0.7671
<i>flexor digitorum superficialis</i>	<i>Accipiter nissus</i>	Bribiesca- Contreras & Sellers, 2017	0.076	74	1.0326
<i>humero-triceps</i>	<i>Accipiter nissus</i>	Bribiesca- Contreras & Sellers, 2017	0.813	839	0.9693

(continued)

Muscle	Species	Study	Mass (g)	diceCT Volume (mm ³)	Muscle Density (g/cm ³)
<i>interosseus dorsalis</i> (ISD)	<i>Accipiter nisus</i>	Bribiesca-Contreras & Sellers, 2017	0.028	42	0.6739
<i>interosseus ventralis</i> (ISV)	<i>Accipiter nisus</i>	Bribiesca-Contreras & Sellers, 2017	0.028	24	1.1792
Not clear (ECR)	<i>Accipiter nisus</i>	Bribiesca-Contreras & Sellers, 2017	0.486	461	1.0539
<i>pronator profundus</i>	<i>Accipiter nisus</i>	Bribiesca-Contreras & Sellers, 2017	0.275	319	0.8635
<i>pronator superficialis</i>	<i>Accipiter nisus</i>	Bribiesca-Contreras & Sellers, 2017	0.107	125	0.8528

(continued)

Muscle	Species	Study	Mass (g)	diceCT Volume (mm ³)	Muscle Density (g/cm ³)
<i>scapulotriceps</i>	<i>Accipiter nissus</i>	Bribiesca- Contreras & Sellers, 2017	0.297	274	1.0846
<i>supinator</i>	<i>Accipiter nissus</i>	Bribiesca- Contreras & Sellers, 2017	0.019	63	0.2995
<i>tensor propatagialis pars longa (TPLA)</i>	<i>Accipiter nissus</i>	Bribiesca- Contreras & Sellers, 2017	0.370	311	1.1891
<i>ulnometacar palis dorsalis (UMD)</i>	<i>Accipiter nissus</i>	Bribiesca- Contreras & Sellers, 2017	0.102	102	0.9989
<i>ulnometacar palis ventralis (UMV)</i>	<i>Accipiter nissus</i>	Bribiesca- Contreras & Sellers, 2017	0.059	67	0.8871

Note. Some muscles from Bribiesca-Contreras & Sellers (2017) did not match up correctly in terms of abbreviations found within the paper. As such, the closest abbreviation was used, and that muscle was recorded in the table. All quantitative data is still properly correlated, only the name of the muscle may be misidentified.

Table 6

Muscle density one sample *t* test results

	Mean										
	Density	SD	N*	<i>t</i> *	df*	SEM*	p*	<i>t</i> †	df †	SEM †	p †
	(g/cm ³)										
All data	1.0103	0.439	44	0.6966	43	0.066	0.4898	0.7510	43	0.066	0.4568
This study	0.8676	0.248	10	2.4074	9	0.078	0.0394	2.4533	9	0.078	0.0366
Baverstock et al. 2013	0.9636	0.141	6	1.5809	5	0.058	0.1747	1.6747	5	0.058	0.1548
Bribiesca - Contreras & Sellers, 2017	1.0713	0.521	28	0.1696	27	0.098	0.8666	0.1148	27	0.098	0.9095
Mammalian data	0.9036	0.214	16	2.8561	15	0.054	0.0120	2.9234	15	0.054	0.0105

(continued)

	Mean										
	Density (g/cm ³)	SD	N*	<i>t</i> *	df*	SEM*	<i>p</i> *	<i>t</i> †	df †	SEM †	<i>p</i> †
Without outliers	0.9385	0.290	42	2.6348	41	0.045	0.0118	2.7152	41	0.045	0.0096
Bribiesca - Contreras & Sellers, 2017 without outliers	0.9600	0.331	26	1.485	25	0.065	0.1500	1.5405	25	0.065	0.1360

*Note. SD=standard deviation; n=sample size; df= degrees of freedom; SEM=standard error of the mean; p=probability; *tested against 1.0564 g/cm³ (Murphy & Beardsley, 1974); †tested against 1.06 g/cm³ (Mendez & Keys, 1960). Significant results are bolded. Mammalian data=This Study + Baverstock et al. 2013.*

Table 7

Bland Altman analyses results

	All (n=44)	Mammalian (n=16)	Avian (n=28)
Old mean % difference	21.96	24.89	20.55
New mean % difference	13.85	1.85	19.99
Change in mean % difference	-8.11	-23.04	-0.56
Old lower limit 95 %CI	-80.84	-44.00	-98.58
Old upper limit 95 %CI	124.76	93.79	139.68
Old range 95 %CI	205.6	137.792	238.26
New lower limit 95 %CI	-87.06	-54.34	-98.59
New upper limit 95 %CI	114.75	58.03	138.59
New range 95 %CI	201.81	112.37	237.18
Range Change	-3.79	-25.422	-1.08

Note. 95%CI=95% confidence intervals; Mammalian=This study + Baverstock et al. (2013); Avian=Bribiesca-Contreras & Sellers (2017). Bolded results represent changes based on newly calibrated constants.

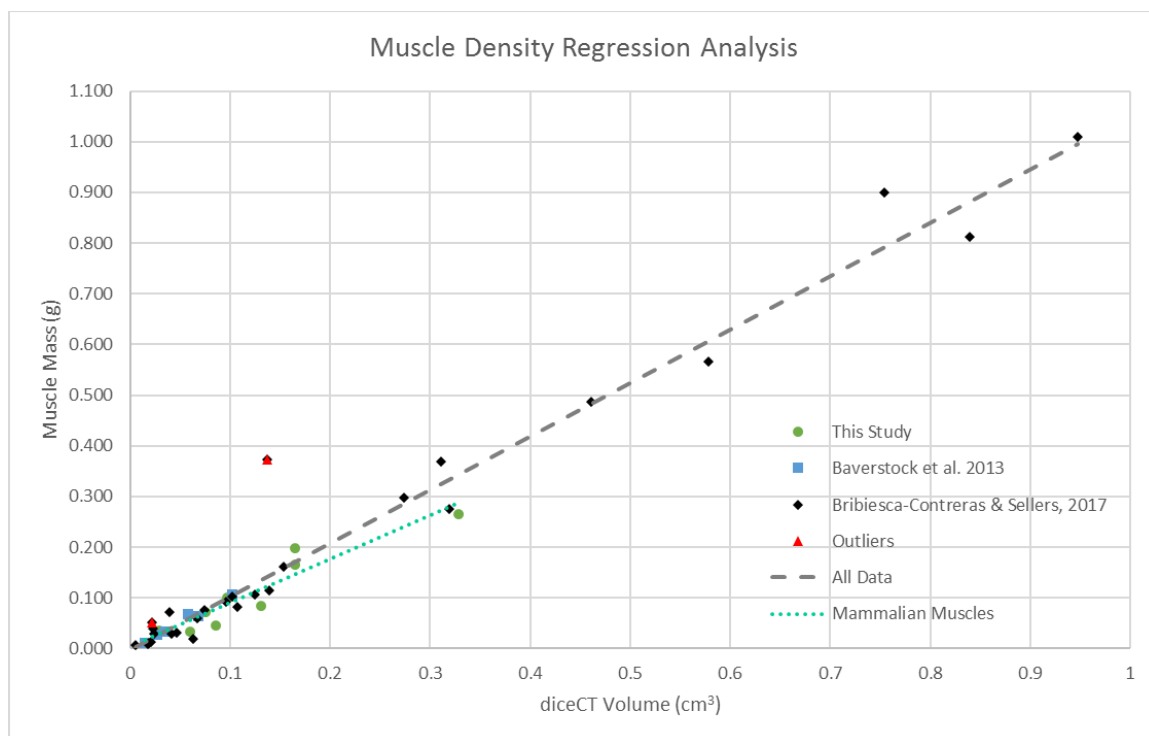


Figure 17. Regression analysis of muscle density data. Data produced by this study is represented by green dots (n=10). Data from Baverstock et al. 2013 is represented by blue squares. Data from Bribiesca-Contreras & Sellers, 2017 is represented by black diamonds, with red triangles overlaying the two outliers discussed in the results. The regression line for all of the data is gray and dashed ($y=1.0555x - 0.0035$; $R^2=0.9614$), while the regression line for just mammalian muscles is represented as a cyan dotted line ($y=0.8644x + 0.0037$; $R^2=0.9136$).

CHAPTER IV

Conclusions

The research presented here sought to test the null hypothesis that diceCT and gross dissection do not produce significantly different measurements. This hypothesis was tested both as a whole and broken into seven subhypotheses. Based on the results of a Bland-Altman analysis using all measurements gathered from diceCT and gross dissection, diceCT and gross dissection measurements are significantly different. This does not support the null hypothesis, though some subhypotheses' results still do support the original null hypothesis. Other subhypotheses also refute the original null hypothesis, while could not be tested enough here to make a conclusion.

The hypothesis regarding connective tissue was one that supported the null hypothesis, as there was no significant difference between gross dissection and diceCT measurements in connective tissue. The hypothesis regarding bone measurements was also supported, though the mandible volume from diceCT was about 20% smaller than those from gross dissection and CT. Linear measurements were also not significantly different between gross dissection and diceCT, supporting the null hypothesis.

Volumetric measurements, muscle measurements, and epithelial measurements were all found to be significantly different between diceCT and gross dissection. Epithelial tissue results were the most different in terms of 95% confidence interval range. Muscle tissues were also significantly different, which was further hypothesized to be due to the use of a constant for mammalian muscle density. This hypothesis was supported as the muscle densities obtained from the *Callithrix jacchus* specimen were significantly different from the previously established values. New constants were

proposed, but suggested to only be used for museum specimens and others that cannot be dissected. Otherwise, muscle density should not be treated as constant, meaning a dissection that gathers mass data should be used in conjunction with diceCT volume information to inform density calculations. Since almost all of the volumetric dataset was comprised of muscle or epithelial volumes, it stands to reason that volumetric measurements were also found to be significantly different.

The hypothesis regarding nervous tissue was unable to be fully explored, as the iodine staining technique seems to have altered the structural integrity tissue making it brittle, leading to difficulties in gross dissection. Similar issues were found with connective tissue being affected due to staining.

Further research regarding the differences between diceCT and gross dissection need to seek to better understand why epithelial and muscle tissue volumes were so different, as the muscle density constant does not explain issues with non-muscles, or those obtained using Archimedes' method. Mammalian muscle tissue density, as well as other taxa, and therefore its effect on diceCT and gross dissections needs to be further analyzed across more species and more taxa. This may also lend itself to phylogenetic studies involving muscles. Nervous tissue also needs to be further observed, as this study was unable to determine if there is a significant difference between gross dissection and diceCT.

REFERENCES

- Albuquerque MA, Gaia BF, Cavalcanti MG.** (2011) Comparison between multislice and cone-beam computerized tomography in the volumetric assessment of cleft palate. *Oral Surg Oral Med Oral Pathol Oral Radiol Endod* **112(2)**, 249-257.
- Akkari N, Enghoff H, Metscher BD.** (2015) A new dimension in documenting new species: High-detail imaging of myriapod taxonomy and first 3D cybertype of a new millipede species (Diplopoda, Julida, Julidae). *PLoS ONE* **10(8)**: e0135243.
- Altman DG, Bland JM.** (1983) Measurement in medicine: The analysis of method comparison studies. *J R Stat Soc* **32**, 307-317.
- Anderson R, Maga AM.** (2015) A novel procedure for rapid imaging of adult mouse brains with microCT using iodine-based contrast. *PLoS ONE* **10(11)**: e0142974.
- Anscombe FJ.** (1973) Graphs in statistical analysis. *The American Statistician* **27**, 17–21.
- Aslandi OV, Nikolaidou T, Zhao J, et al.** (2013) Application of micro-computed tomography with iodine staining to cardiac imaging, segmentation and computational model development. *IEEE Trans Med Imaging* **32(1)**, 8-17.
- Balanoff AM, Bever GS, Colbert MW, et al.** (2015) Best practices for digitally constructing endocranial casts: examples from birds and their dinosaurian cousins. *J Anat* **229**, 173-190.
- Baverstock H, Jeffery NS, Cobb SN** (2013) The morphology of the mouse masticatory musculature. *J Anat* **223**, 46–60.

- Bribiesca-Contreras F, Sellers WI.** (2017) Three-dimensional visualization of the internal anatomy of the sparrowhawk (*Accipiter nisus*) forelimb using contrast-enhanced micro-computed tomography. *PeerJ* **5**: e3039.
- Brown AA, Scarfe WC, Scheetz JP, et al.** (2009) Linear accuracy of cone beam CT derived 3D images. *Angle Orthod* **79**(1), 150-157.
- Buytaert J, Goyens J, De Greef D, et al.** (2014) Volume shrinkage of bone, brain, and muscle tissue in sample preparation for micro-CT and light sheet fluorescence microscopy (LSFM). *Microsc Microanal* **20**, 1208-1217.
- Clarke JA, Chatterjee S, Li Z, et al.** (2016) Fossil evidence of the avian vocal organ from the Mesozoic. *Nature* **538**, 502–505
- Cox PG, Fagan MJ, Rayfield EJ, et al.** (2011) Finite element modeling of squirrel, guinea pig and rat skulls: using geometric morphometrics to assess sensitivity. *J Anat* **219**, 696–709.
- Cox PG, Faulkes CG.** (2014) Digital dissection of the masticatory muscles of the naked mole-rat, *Heterocephalus glaber* (Mammalia, Rodentia). *PeerJ* **2**, e448.
- Cox PG, Jeffery N.** (2011) Reviewing the morphology of the jaw-closing musculature in squirrels, rats, and guinea pigs with contrast-enhanced micro-CT. *Anat Rec* **294**, 915–928.
- Cox PG, Rayfield EJ, Fagan MJ, et al.** (2012) Functional evolution of the feeding system in rodents. *PLoS ONE* **7**, e36299.
- Critchley LAH, Critchley AJH.** (1999) A meta-analysis of studies using bias and precision statistics to compare cardiac output measurement techniques. *J Clin Monit Comput* **15**(2), 85-91.

- Damstra J, Fourie Z, Huddleston Slater JJR, et al.** (2010) Accuracy of linear measurements from cone-beam computed tomography-derived surface models of different voxel sizes. *Am J Orthod Dentofacial Orthop* **137**, 16.e1-16.e6.
- Davis GR, Wong FS.** (1996) X-ray microtomography of bone and teeth. *Physiol Meas* **17**, 121-146.
- Degenhardt K, Wright AC, Horng D, et al.** (2010) Rapid 3D phenotyping of cardiovascular development in mouse embryos by micro-CT with iodine staining. *Circ Cardiovasc Imaging* **2010(3)**, 314-322.
- Dickinson E, Stark H, Kupczik K.** (2018) Non-destructive determination of muscle architectural variables through the use of diceCT. *Anat Rec* **301**, 363-377.
- Dougherty LR, Rahman IA, Burdfield-Steel ER, et al.** (2015) Experimental reduction of intromittent organ length reduces male reproductive success in a bug. *Proc Roy Soc Lond B* **282**, 20150724
- Düring DN, Ziegler A, Thompson CK, et al.** (2013) The songbird syrinx morphome: a three-dimensional, high-resolution, interactive morphological map of the zebra finch vocal organ. *BMC Biol* **11**, 1.
- Dusseldorp JK, Stamatakis HC, Ren Y.** (2017) Soft tissue coverage on the segmentation accuracy of the 3D surface-rendered model from cone-beam CT. *Clin Oral Invest* **21**, 921-930.
- Elliot JC, Dover SD.** (1982) X-ray microtomography. *J Microsc* **126(2)**, 211-213.
- Eng CM, Ward SR, Vinyard CJ, Taylor AB.** (2009) The morphology of the masticatory apparatus facilitates muscle force production at wide jaw gaps in

tree-gouging common marmosets (*Callithrix jacchus*). *J Exp Biol* **212**, 4040-4055.

- Faulwetter S, Vasileiadou A, Kouratoras M, et al.** (2013) Micro-computed tomography: Introducing new dimensions to taxonomy. *Zookeys* **263**, 1-45.
- Fernández R, Kvist S, Lenihan J, et al.** (2014) Sine systemate chaos? A versatile tool for earthworm taxonomy: non-destructive imaging of freshly fixed and museum specimens using micro-computed tomography. *PLoS ONE* **9**, e96617.
- Fleagle JG.** (2013) Primate adaptation and evolution. 3rd ed. New York: Academic Press.
- Gans C.** (1982) Fiber architecture and muscle function. *Exerc Sport Sci Rev* **10**, 160-207
- Giavarina D.** (2015) Understanding Bland Altman analysis. *Biochem Med (Zagreb)* **25(2)**, 141-151.
- Gignac PM, Kley NJ.** (2014) Iodine-enhanced micro-CT imaging: Methodological refinements for the study of soft-tissue anatomy of post-embryonic vertebrates. *J Exp Zool B Mol Dev Evol* **322B**, 166-176.
- Gignac PM, Kley NK, Clarke JA, et al.** (2016) Diffusible iodine-based contrast-enhanced computed tomography (diceCT): an emerging tool for rapid, high-resolution, 3-D imaging of metazoan soft tissues. *J Anat* **228**, 889–909.
- Güngör E, Doğan MS.** (2017) Reliability and accuracy of cone-beam computed tomography voxel density and linear distance measurement at different voxel sizes: a study on sheep head cadaver. *J Dent Sci* **12**, 145-150.
- Hartstone-Rose A, Deutsch AR, Leischner CL, et al.** (2018) Dietary correlates of primate masticatory muscle fiber architecture. *Anat Rec* **301(2)**, 311-324.

- Hartstone-Rose A, Perry JMG, Morrow CJ.** (2012) Bite force estimation and the fiber architecture of felid masticatory muscles. *Anat Rec* **295**, 1336-1351.
- Hautier L, Lebrun R, Cox PG.** (2012) Patterns of covariation in the masticatory apparatus of hystricognathous rodents: implications for evolution and diversification. *J Morphol* **273**, 1319–1337.
- Herdina AN, Herzig-Straschil B, Hilgers H, et al.** (2010) Histomorphology of the penis bone (baculum) in the gray long-eared bat *Pleocotus austriacus* (Chiroptera, Vespertilionidae). *Anat Rec* **293**, 1248–1258.
- Herdina AN, Kelly DA, Jahelková H, et al.** (2015a) Testing hypotheses of bat baculum function with 3-D models derived from micro-CT. *J Anat* **226**, 229–235.
- Herdina AN, Plenk Jr. H, Benda P, et al.** (2015b) Correlative 3D-imaging of *Pipistrellus* penis micromorphology: Validating quantitative microCT images with undecalcified serial ground section histomorphology. *J Morphol* **276**, 695–706.
- Herrel A, De Smet A, Aguire LF, Aerts P.** (2008) Morphological and mechanical determinants of bite force in bats: do muscles matter? *J Exp Biol* **211**, 86-91
- Holliday CM, Tsai HP, Skiljan RJ, et al.** (2013) A 3-D interactive model and atlas of the jaw musculature of *Alligator mississippiensis*. *PLoS ONE* **8**, e62806.
- Hughes DF, Gignac PM, Walker EM, et al.** (2016) Rescuing perishable neuroanatomical information from a threatened biodiversity hotspot: Remote field methods for brain tissue preservation validated by semi-quantitative cytoarchitectonic analysis, immunohistochemistry, and iodine-enhanced X-ray microcomputed tomography. *PLoS ONE* **11(5)**, e0155824.

- Jeffrey NS, Stephenson RS, Gallagher JA, et al.** (2011) Micro-computed tomography with iodine staining resolves the arrangement of muscle fibres. *J Biomech* **44**, 189-192.
- Kupczik K, Stark H, Mundry R, et al.** (2015) Reconstruction of muscle fascicle architecture from iodine-enhanced microCT images: A combined texture mapping and streamline approach. *J Theor Biol* **382**, 34-43.
- Lagravere MO, Carey J, Toogood RW, et al.** (2008) Three-dimensional accuracy of measurements made with software on cone-beam computed tomography images. *Am J Orthod Dentofacial Orthop* **134(1)**, 112-116.
- Lautenschlager S, Bright JA, Rayfield EJ.** (2013) Digital dissection—using contrast-enhanced computed tomography scanning to elucidate hard- and soft-tissue anatomy of the Common Buzzard *Buteo buteo*. *J Anat* **224**, 412–431.
- Leischner CL, Crouch M, Allen KL, et al.** (2018) Scaling of primate forearm muscle architecture as it relates to locomotion and posture. *Anat Rec* **301(3)**, 484-495.
- Li Z, Clarke JA, Ketcham RA, et al.** (2015) An investigation of the efficacy and mechanism of contrast-enhanced x-ray computed tomography utilizing iodine for large specimens through experimental and simulation approaches. *BMC Physiol* **15**, 5, 16pp.
- Li Z, Ketcham RA, Yan F, et al.** (2016) Comparison and evaluation of the effectiveness of two approaches of diffusible iodine-based contrast- enhanced computed tomography (diceCT) for avian cephalic material. *J Exp Zool B Mol Dev Evol* **00B**, 1–11.

- Loubele M, Maes F, Schutyser F, et al.** (2006) Assessment of bone segmentation quality of cone-beam CT versus multislice spiral CT: a pilot study. *Oral Surg Oral Med Oral Pathol Oral Radiol Endod* **102**(2), 225-234.
- Ludbrook J.** (1997) Comparing methods of measurements. *Clin Exp Pharmacol Physiol* **24**(2), 193-203.
- Maret D, Peters OA, Galibourg A, et al.** (2014) Comparison of the accuracy of 3-dimensional cone-beam computed tomography and micro-computed tomography reconstructions by using different voxel sizes. *J Endod* **39**, 394-397.
- Maret D, Telmon N, Peters OA, et al.** (2012) Effect of voxel size on the accuracy of 3D reconstructions with cone beam CT. *Dentomaxillofac Radiol* **41**, 649-655.
- Mendez J, Keys A.** (1960) Density and composition of mammalian muscle. *Metabolism* **9**, 184-188.
- Metscher BD.** (2009a) Micro-CT for developmental biology: a versatile tool for high-contrast 3-D imaging at histological resolutions. *Dev Dyn* **238**, 632–640.
- Metscher BD.** (2009b) Micro-CT for comparative morphology: simple staining methods allow high-contrast 3D imaging of diverse non-mineralized animal tissues. *BMC Physiol* **9**, 11.
- Metscher BD.** (2013) Biological applications of X-ray microtomography: imaging micro-anatomy, molecular expression and organismal diversity. *Micros Anal* **27**, 13–16.
- Miller MN.** (1898) Students histology: a course of normal histology for students and practitioners of medicine. 3rd ed. New York: William Wood & Company.
- Mizutani R, Suzuki Y.** (2012) X-ray microtomography in biology. *Micron* **43**, 104-115.

- Moerenhout BA, Gelaude F, Swennen GRJ, et al.** (2009) Accuracy and repeatability of cone-beam computed tomography (CBCT) measurements used in the determination of facial indices in the laboratory setup. *J Craniomaxillofac Surg* 37(1), 18-23.
- Murphy RA, Beardsley AC.** (1974) Mechanical properties of the cat soleus muscle in situ. *Am J Physiol* 227(5), 1008-1013
- Neues F, Goerlich R, Renn J, et al.** (2007) Skeletal deformations in medaka (*Oryzias latipes*) visualized by synchrotron radiation micro-computer tomography (SRmicroCT). *J Struct Biol* 160, 236-240.
- Otten E.** (1988) Concepts and models of functional architecture in skeletal muscle. *Exerc Sport Sci Rev* 16, 98-138.
- Pauwels E, Van Loo D, Cornillie P, et al.** (2013) An exploratory study of contrast agents for soft tissue visualization by means of high resolution X-ray computed tomography imaging. *J Microsc* 250, 21-31.
- Periago DR, Scarfe WC, Moshiri M, et al.** (2008) Linear accuracy reliability of cone beam CT derive 3-dimensional images constructed using an orthodontic volumetric rendering program. *Angle Orthod* 78(3), 387-395.
- Perry JMG, Hartstone-Rose A, Wall CE.** (2011) The jaw adductors of strepsirrhines in relation to body size, diet, and ingested food size. *Anat Rec* 294, 712-728.
- Perry JMG, Macneill KE, Heckler AL, et al.** (2014) Anatomy and adaptations of the chewing muscles in *Daubentonia* (Lemuriformes). *Anat Rec* 297, 308-316.
- Peters OA, Laib A, Rügsegger P.** (2000) Three-dimensional analysis of root canal geometry by high-resolution computed tomography. *J Dent Res* 79(6), 1405-1409.

- Pinheiro HLN and Pontes ARM.** (2015) Home range, diet, and activity patterns of common marmosets (*Callithrix jacchus*) in very small and isolated fragments of the Atlantic forest of northeastern Brazil. *International Journal of Ecology* **2015** 685816.
- Ramírez MJ, Coddington JA, Maddison WP, et al.** (2007) Linking of Digital Images to Phylogenetic Data Matrices Using a Morphological Ontology. *Syst Biol* **56(2)**, 283-294.
- Rupert JE, Rose JA, Organ JM, Butcher MT.** (2015) Forelimb muscle architecture and myosin isoform composition in the groundhog (*Marmota monax*). *J Exp Biol* **218**, 194-205.
- Rylands AB, Coimbra-Filho AF, Mittermeier RA.** (1993) Systematics, geographic distribution, and some notes on the conservation status of the Callitrichidae. In Rylands AB (ed), *Marmosets and tamarins: systematics, behaviour, and ecology*. Oxford University Press, Oxford, 11-77.
- Rylands AB, Mittermeier RA, de Oliveira MM, et al.** (2008) *Callithrix jacchus*. The IUCN Red List of Threatened Species **2008**: e.T41518A10485463.
- Sang Y-H, Hu H-C, Lu S-H, et al.** (2016) Accuracy assessment of three-dimensional surface reconstructions of in vivo teeth from cone-beam computed tomography. *Chin Med J (Engl)* **129(12)**, 1464-1470.
- Santana SE.** (2018) Comparative anatomy of bat jaw musculature via diffusible iodine-based contrast-enhanced computed tomography. *Anat Rec* **301**: 267-278.
- Santana SE, Dumont ER, Davis JL.** (2010) Mechanics of bite force production and its relationship to diet in bats. *Funct Ecol* **24**, 776-784.

- Seymour KL.** (1999) Taxonomy, morphology, paleontology and phylogeny of the South American small cats (Mammalia: Felidae). University of Toronto Ph.D. Thesis.
- Shaheen E, Khalil W, Ezeldeen M, et al.** (2017) Accuracy of segmentation of tooth structures using 3 different CBCT machines. *Oral Surg Oral Med Oral Pathol Oral Radiol* **123**(1), 123-128.
- Sombke A, Lipke E, Michalik P, et al.** (2015) Potential and limitations of X-Ray micro-computed tomography in arthropod neuroanatomy: A methodological and comparative survey. *J Comp Neurol* **523**, 1281-1295.
- Staedler YM, Masson D, Schönenberger J.** (2013) Plant tissues in 3D via x-ray tomography: Simple contrasting methods allow high resolution imaging. *PLoS ONE* **8**(9): e75295
- Stephenson RS, Boyett MR, Hart G, et al.** (2012) Contrast enhanced micro-computed tomography resolves the 3-dimensional morphology of the cardiac conduction system in mammalian hearts. *PLoS ONE* **7**(4), e35299.
- Tahara R, Larsson HCE.** (2013) Quantitative analysis of microscopic X-ray computed tomography imaging: Japanese quail embryonic soft tissues with iodine staining. *J Anat* **223**, 297-310.
- Taylor AB, Eng CM, Anapol F, Vinyard C.** (2009) The functional correlates of jaw-muscle fiber architecture in tree-gouging and nongouging callitrichid monkeys. *Am J Phys Anthropol* **139**, 353-367.
- Taylor A, Vinyard C.** (2004) Comparative analysis of masseter fiber architecture in tree-gouging (*Callithrix jacchus*) and nongouging (*Saguinus oedipus*) callitrichids. *J Morphol* **261**, 276-285.

- Tsai HP, Holliday CM.** (2011) Ontogeny of the alligator cartilage transiliens and its significance for sauropsid jaw muscle evolution. *PLoS ONE* **6(9)**, e24935.
- Vasquez SX, Hansen MS, Bahadur AN, et al.** (2008) Optimization of volumetric computed tomography for skeletal analysis of model genetic organism *Anat Rec* **291**, 475-487.
- Vickerton P, Jarvis J, Jeffery N.** (2013) Concentration-dependent specimen shrinkage in iodine-enhanced microCT. *J Anat* **223**, 185-193.
- Vickerton P, Jarvis J, Gallagher JA, et al.** (2014) Morphological and histological adaptation of muscle and bone to loading induced by repetitive activation of muscle. *Proc Roy Soc B* **281**, 20140786.
- Whyms BJ, Vorperian HK, Gentry LR, et al.** (2013) The effect of CT scanner parameters and 3D volume rendering techniques on the accuracy of linear, angular, and volumetric measurements of the mandible. *Oral Surg Oral Med Oral Pathol Oral Radiol* **115(5)**, 682-691.
- Wong MD, Dorr AE, Walls JR, et al.** (2012) A novel 3-D mouse embryo atlas based on micro-CT. *Development* **129**, 3248–3256.
- Wong MD, Maezawa Y, Lerch JP, et al.** (2014) Automated pipeline for anatomical phenotyping of mouse embryos using micro-CT. *Development* **141**, 2533-2541.
- Wong MD, Spring S, Henkelman RM.** (2013) Structural stabilization of tissue for embryo phenotyping using micro-CT with iodine staining. *PLoS ONE* **8**, e84321.
- Yuen AHL, Tsui HCL, Kot BCW.** (2017) Accuracy and reliability of cetacean cranial measurements using computed tomography three dimensional volume rendered images. *PLoS ONE* **12(3)**, e0174215.

Zimmermann D, Randolph S, Metscher BD, et al. (2011) The function and phylogenetic implications of the tentorium in adult Neuroptera (Insecta). *Arthropod Struct Dev* **40**, 571-582.

APPENDIX

Material Statistics from Amira 5.6

Material	Count (voxels)	Volume (mm ³)	CenterX	CenterY	CenterZ	Mean GV	Deviation n	Variance	Min GV	Max GV	CumulativeSum
Exterior	3,780,456,192	63425.5313	19.8784	19.4443	24.0272	40.8750	23.0077	529.3524	0	255	154,526,203,904.00
Superficial Masseter (Right)	10,525,693	176.5918	9.6698	29.9481	25.5544	86.3457	12.9820	168.5315	47	139	908,848,320.00
Deep Masseter (Right)	3,592,418	60.2708	9.4737	28.1952	24.0928	84.3967	11.1040	123.2987	48	130	303,188,128.00

(continued)

Material	Count (voxels)	Volume (mm ³)	CenterX	CenterY	CenterZ	Mean GV	Deviation n	Variance	Min GV	Max GV	Cumulative Sum
Zygomat ico- mandibul aris (Right)	4,752,57 1	79.7349	8.7379	25.3521	24.3248	78.5424	11.4134	130.2657	45	120	373,278, 272.00
Deep Medial Pterygoid (Right)	4,052,21 9	67.9850	12.6120	28.7528	26.8182	82.8608	11.4089	130.1639	45	122	335,770, 048.00
Superfici al Medial Pterygoid (Right)	2,491,62 3	41.8025	12.0755	26.8112	26.7842	80.1559	12.0084	144.2008	42	119	199,718, 320.00
Lateral Pterygoid (Right)	4,226,61 8	70.9109	12.2761	22.9013	24.9252	80.1925	12.0990	146.3867	42	114	338,943, 232.00

(continued)

Material	Count (voxels)	Volume (mm ³)	CenterX	CenterY	CenterZ	Mean GV	Deviation n	Variance	Min GV	Max GV	Cumulative Sum
Temporalis (Right)	45,363,4 20	761.0719	7.8399	14.9591	24.1277	76.9459	12.0973	146.3440	43	255	3,490,52 6,976.00
Posterior Digastric (Left)	874,884	14.6781	26.8096	23.0269	36.0357	78.6371	12.0677	145.6293	37	115	68,798,2 96.00
Medial Pterygoid (Left)	7,778,96 2	130.5093	25.9452	28.2862	26.0453	77.2014	13.2224	174.8327	40	120	600,546, 560.00
Parotid Gland (Right)	12,019,5 70	201.6549	7.3821	25.7236	31.5701	73.9516	8.2404	67.9048	42	116	888,866, 688.00

(continued)

Material	Count (voxels)	Volume (mm ³)	CenterX	CenterY	CenterZ	Mean GV	Deviation n	Variance	Min GV	Max GV	Cumulative Sum
Submandibular Gland (Right)	8,448,001	141.7339	12.6453	32.6662	35.4543	79.4965	6.6320	43.9829	48	116	671,586,368.00
Whisker (Right)	12,336	0.2070	7.2550	24.0723	5.5173	59.0751	33.4012	1115.6431	20	183	728,750.00
Digastric (Right)	2,991,666	50.1918	14.5982	30.1588	26.4556	81.8930	14.5180	210.7729	39	127	244,996,448.00
Lens (Left)	857,100	14.3798	23.2632	17.9533	12.6642	71.4262	7.0512	49.7188	48	96	61,219,368.00

(continued)

Material	Count (voxels)	Volume (mm ³)	CenterX	CenterY	CenterZ	Mean GV	Deviatio n	Variance	Min GV	Max GV	Cumulati veSum
Deep Tempora lis (Left)	19,568,9 40	328.3123	29.0766	14.0531	24.7379	82.8967	12.5192	156.7296	32	134	1,622,20 0,576.00
Zygomat ico- mandibul aris (Left)	5,785,10 0	97.0579	29.0490	25.2347	22.8201	80.0422	12.6257	159.4090	44	126	463,051, 936.00
Deep Masseter (Left)	3,572,04 7	59.9290	28.6283	27.9096	22.8767	85.3360	11.8867	141.2929	45	128	304,824, 256.00
Superfici al Masseter (Left)	9,849,48 1	165.2469	28.1194	30.2610	24.7922	86.5708	13.3279	177.6330	44	134	852,677, 952.00

(continued)

Material	Count (voxels)	Volume (mm ³)	CenterX	CenterY	CenterZ	Mean GV	Deviation n	Variance	Min GV	Max GV	CumulativeSum
Superficial Temporalis (Left)	9,849,80 1	165.2522	30.2495	14.1500	22.0590	84.3411	11.5955	134.4565	44	254	830,743, 040.00
Zygomatic Temporalis (Left)	5,102,07 0	85.5985	30.8915	22.0302	22.6646	76.4912	13.3144	177.2719	42	123	390,263, 712.00
Lateral Pterygoid (Left)	4,484,86 4	75.2435	25.7624	22.9196	24.5118	78.0309	12.8172	164.2814	41	117	349,957, 792.00
Anterior Digastric (Left)	1,746,34 6	29.2988	21.8798	33.7710	20.2230	84.4946	13.5695	184.1303	44	127	147,556, 720.00

(continued)

Material	Count (voxels)	Volume (mm ³)	CenterX	CenterY	CenterZ	Mean GV	Deviation n	Variance	Min GV	Max GV	CumulativeSum
Lens (Right)	836,834	14.0397	10.1890	18.1146	13.1972	71.9118	5.9377	35.2560	45	93	60,178,2 16.00
Sublingual Gland (Left)	1,293,938	21.7087	22.7925	32.7635	28.3423	67.5470	5.1808	26.8409	47	98	87,401,6 80.00
Mandible	24,347,104	408.4766	18.8736	30.7307	16.9854	79.5130	11.9534	142.8834	54	187	1,935,91 1,808.00

Note. GV=Grayscale values; Center represents the coordinates of the centroid of the segmented material.

VITA

Curriculum Vitae

August 2018

Justin Levy

Sam Houston State University

Department of Biological Sciences

EDUCATION

Missouri University of Science and Technology (Missouri S&T), Rolla, Missouri

B.S. May 2015 (Geology and Geophysics)

Minor May 2015 (Global Studies)

Sam Houston State University, Huntsville, Texas (Advisor: Patrick J. Lewis)

M.S. *in progress* (Biology)**RESEARCH INTERESTS**

Historical ecology

Anthropogenic forces on mammalian and avian populations

Applied anthropology

HONORS, ELECTED POSITIONS, & AWARDS

Missouri Miner Scholarship, Missouri S&T, 2010-11.

Bright Flight Scholarship, Missouri S&T, 2010-12.

Access Missouri Scholarship, Missouri S&T, 2010-15.

Tacachia, Bolivia Distribution System Project Lead, Engineers Without Borders,
Missouri S&T, 2010-12.

Tacachia, Bolivia Public Relations Chair, Engineers Without Borders, Missouri
S&T, 2010-11, 2014-15

Engineers Without Borders-S&T Chapter Fundraising Chair, Executive Board,
Engineers Without Borders, Missouri S&T, 2011-12.

Radcliffe Scholarship, Missouri S&T, 2011, 2014-15.

Tacachia, Bolivia Fundraising Chair, Engineers Without Borders, Missouri S&T,
2012-15.

Starting Defenseman and Executive Board Member, Missouri S&T Lacrosse
Club, Missouri S&T, 2012-2015.

James Redding Geology Scholarship, Missouri S&T, 2012-13.

Kerry Grant Geology Field Camp Scholarship, Missouri S&T, 2013.

Weiner Scholarship for International Study Abroad, Missouri S&T, 2013-14.

V.H. McNutt Geology Scholarship, Missouri S&T, 2013-14.

Gavin Bradford Donohue Memorial Scholarship for Outstanding Contributions to
Engineers Without Borders, Missouri S&T, 2013-14.

Student Ambassador for Incoming Exchange Students, International Student
Club, Missouri S&T, Fall 2014.

Academy of Mines & Metallurgy Geology and Geophysics Academy Scholar,
Missouri S&T, 2015.

Sigma Gamma Epsilon (Earth Sciences Honor Society), Missouri S&T, 2014-15.

College of Sciences Special Graduate Scholarship, Sam Houston State University,
2016.

College of Science and Engineering Technology Special Graduate Scholarship,
Sam Houston State University, 2017.

GRANTS

Levy, J. and Hoff, R. 2011. Engineers Without Borders Water Supply and Water
Quality Project in Nahualate, Guatemala, GeoEngineering Grant. **\$3,000**

Levy, J. 2011-2012. Engineers Without Borders Water Supply and Water Quality
Project in Nahualate, Guatemala, St. Louis Gateway Professionals EWB
Chapter Grant. **\$750**

Levy, J. and Pherigo, C. 2012-2013. Engineers Without Borders Distribution
System, Water Quality and Erosional Control Project in Tacachia, Bolivia,
Boeing Grant. **\$4,000**

Pherigo, C., Hoff, R. and Levy, J. 2012-2013. Engineers Without Borders Water
Supply and Water Quality Project in Nahualate, Guatemala, ARCO
Construction Grant. **\$10,000**

Pherigo, C. and Levy, J. 2012-2013. Engineers Without Borders Water Supply
and Water Quality Project in Nahualate, Guatemala, St. Louis Gateway
Professionals EWB Chapter Grant. **\$750**

Pherigo, C. and Levy, J. 2013. Engineers Without Borders Water Supply and
Water Quality Project in Nahualate, Guatemala, Ameren Grant. **\$5,000**

Levy, J. 2016. Travel Grant to Present Research, Sam Houston State University.
\$1,200

Total Grant Money Received: **\$24,700**

PRESENTATIONS

Jenkins, K., **J. Levy**, K. Bergstrom, R. J. Velasquez, P. J. Lewis, and T.

Campbell. 2016. Use of computed tomography survey to reveal hidden
structures and a survey of supernumerary molars within *Pongo pygmaeus*.

Texas Academy of Science Annual Meeting, Junction, TX. (3-4 March
2016)

Bergstrom, K., K. Jenkins, **J. Levy**, R. J. Velasquez, P. Lewis, and T. Campbell.

2016. Computed tomography survey of supernumerary molars in extant
orangutans with implications for studies of the primate fossil record.

Paleoanthropological Society Annual Meeting, Atlanta, GA. (12-13 April
2016)

Levy, J., Z. W. Pierce, M. C. Vallejo-Pareja, and P. J. Lewis. 2016. A new

interpretation of fossil muskrat species using lower first molar
morphology. *Evolution* 2016, Austin, TX. (17-21 June 2016)

- Levy, J., C. Fakhri, P. J. Lewis, and A. Hartstone-Rose.** 2016. Relationship of masseter volume to diet in different cebids. American Society of Mammalogists Annual Meeting, Minneapolis, MN. (24-28 June 2016)
- Levy, J., Z. W. Pierce, M. C. Vallejo-Pareja, and P. J. Lewis.** 2016. One, two, or six? Rethinking fossil muskrat taxonomy using molar morphology. Rodens et Spatium 2016, Olomouc, Czech Republic. (25-29 July 2016)
- Pierce, Z. W., J. Levy, M. C. Vallejo-Pareja, and P. J. Lewis.** 2016. To lump or not to lump? Analyzing fossil muskrat taxonomy using molar morphology. Society of Vertebrate Paleontology 76th Annual Meeting, Salt Lake City, UT. (26-29 October 2016)
- Levy, J., R. W. Burroughs, Z. W. Pierce, M. C. Vallejo-Pareja, and P. J. Lewis.** 2016. A rigid palm tree or a mighty branching oak? Using muskrats to study evolutionary mode. Society of Vertebrate Paleontology 76th Annual Meeting, Salt Lake City, UT. (26-29 October 2016)
- Levy, J., P. J. Lewis, and A. Hartstone-Rose.** 2016. A comparison of measurements in analog and digital dissection. Texas Association of Biological Anthropologists 10th Annual Meeting, Austin, TX. (18-19 November 2016)
- Levy, J., P. J. Lewis, and A. Hartstone-Rose.** 2017. A quantitative analysis of iodine stained CT (DiceCT) measurements in physical and digital dissection. American Association of Physical Anthropologists 86th Annual Meeting, New Orleans, LA. (19-22 April 2017)

RELEVANT EXPERIENCE

PROFESSIONAL APPOINTMENTS

United States Geological Survey, Missouri Water Science Center, Rolla, MO. June 2014-May 2015. Pathways Hydrology Intern and Junior Lab Technician in Sediment Lab.

TEACHING APPOINTMENTS

Missouri S&T, Department of Geosciences and Geological and Petroleum Engineering (GGPE), Rolla, MO. Aug 2014-Dec 2014. Teaching Assistant for Industrial and Metallic Ore Deposits.

Sam Houston State University, Department of Biological Sciences, Huntsville, TX. Teaching Assistantship, Aug 2015-May 2017. Courses: Botany, Zoology, Human Physiology.

Waller High School, Science Department, Waller, TX. Teacher and Debate Coach, Aug 2017-Present. Courses: Chemistry, Aquatic Science.

FIELD WORK

May 2011: Engineers Without Borders Distribution System, Water Quality and Erosional Control Project. Tacachia, Bolivia (small rural community in the Andes Mountains). Leader of Distribution Team. In charge of design and construction of a potable water

distribution system, including settling tanks, storage tanks, ram pumps, and piping.

May-June 2012: Missouri S&T Field Geology. Rolla, MO, Arbuckle Mountains of OK, Dallas, TX, and the Picuris Mountains of NM. Emphasis on basic geologic concepts, fundamental field skills including logistical planning, navigation, data collection and documentation and mapping.

May-June 2013: Missouri S&T Advanced Field Geology. Cedar City, UT, surrounding areas, including the Red Hill, Kolob Canyon, and Parowan Gap. Emphasis on structural geology, igneous and metamorphic geology, sedimentary geology, and mapping.

October 2013: Fieldwork with Missouri S&T. Cypress Pond, MO. Took several meters of lake cores to be used in palynological studies for doctoral research of R. Haselwander.

May 2015: Missouri S&T Geological Field Studies. Gerace Research Centre, San Salvador, Bahamas. Emphasis on investigating interactions between biological and geological systems in the formation of the Bahamian platform and islands.

SERVICE & OUTREACH

St. Louis Science Center National Engineers' Week, 2011. Presenter for

Engineers Without Borders, St. Louis, MO. (26-27 February 2011)

C.L. Dake Geological Society Annual Rock & Mineral Auction, 2011.

Auctioneer, Rolla, MO. (6 November 2011)

St. Louis Science Center Engineering Career Day, 2012. Presenter for Engineers

Without Borders, St. Louis, MO. (6 October 2012)

St. Louis Science Center National Engineers' Week, 2013. Presenter for

Engineers Without Borders, St. Louis, MO. (23-24 February 2013)

Merit Badge University at Missouri S&T, 2015. Geology Merit Badge Instructor,

Rolla, MO. (7 February 2015)

Sam Houston State University 2016 Undergraduate Research Symposium.

Moderator, Huntsville, TX. (23 April 2016)

CURRENT PROFESSIONAL AFFILIATIONS

American Association of Physical Anthropologists

American Society of Mammalogists

American Society of Naturalists

Geological Society of America

Paleontological Society

Society of Vertebrate Paleontology

Texas Academy of Sciences